Nationaal Lucht- en Ruimtevaartlaboratorium
National Aerospace Laboratory NLR

NLR-TP-99256

Frequency domain unsteady aerodynamics in/from aeroelastic simulation

M.H.L. Hounjet, B.B. Prananta and B.J.G. Eussen

Nationaal Lucht- en Ruimtevaartlaboratorium
National Aerospace Laboratory NLR

NLR-TP-99256

Frequency domain unsteady aerodynamics in/from aeroelastic simulation

M.H.L. Hounjet, B.B. Prananta and B.J.G. Eussen

This report is based on a presentation held at the CEAS/AIAA/ICASE/NASA Langley International Forum on Aeroelasticity and Structural Dynamics, Williamsburg, Virginia, U.S.A., 22-25 June 1999.

Division:	Fluid Dynamics
Issued:	June 1999
Classification of title:	unclassified

Summary

Temporal integration schemes are introduced and described which are readily embedded in any time-accurate simulation method and are aiming at an enhanced 'frequency' domain usage of CUA methods. The schemes are categorized as two samples per cycle and one sample per cycle algorithms which refer to the number of samples used to describe a complete cycle. Recent experience with the embedding of one sample per cycle and two samples per cycle algorithms in the AESIM method is presented and discussed.

Keywords Aeroelastic simulation, temporal integration

Contents

(48 pages in total)

1 Introduction

Common practice and realistic prediction of the flutter envelope including nonlinear conditions is an increasingly important aspect of the modern multi-disciplinary aircraft design and analysis process.

When such conditions occur, for instance at transonic flight, at high angles of attack or in case of structural nonlinearities , aeroelastic time-accurate CFD simulation of the behavior of the flexible aircraft is a necessary complement to conventional linear methods.

However, the deployment of time-accurate CFD methods requires additional activities to be carried out such as (dynamic) grid generation and signal analysis and raises the issue of affordability due to its CPU requirements.

The state-of-art in time-accurate CFD has reached a high level of maturity [Pra99] and one should not be to optimistic in expecting much increase of efficiency for the time-accurate CFD solvers. We have demonstrated [PHZ98] that adequate results can be obtained with the Euler equations using 8 time steps per cycle for forced and coupled motions on a dynamic grid. Still the turn-around-time is much higher compared to the linear panel methods and the transonic full potential field panel methods developed in the early eighties. The latter require a few seconds running time on current generation of PC's.

Therefore the affordability of these methods should be increased by developing efficient strategies with respect to their usage. In [HES97] we introduced a MIMO based analysis approach which minimizes the number of simulations and in [PH97] we introduced efficient coupling algorithms, e.g. the prognostic coupling.

Aeroelastic stability analysis involving the use of CUA methods is usually performed with one of the following two strategies:

1. **pk- method (eigenvalue) analysis.** The aerodynamic data (generalized forces in frequency domain) required for these methods might be supplied by:
   - sinusoidal excitation in time domain.
   - impulse excitation in time domain.
   - frequency domain methods.

   The first one is efficient when the state space is relatively small. The second one is more efficient as compared to the first one but requires experience. The latter method is based

on a linearized form of the equations and formulated in complex variables it is known to be limited in frequency range. This problem can be overcome by the diverging rate formulation which has been introduced in [Hou86] and extensively applied in subsonic, transonic and supersonic flow [HE91, HE92].

2. **Fully-coupled simulation**. This method is especially useful in case of strong nonlinearities and a large number of vibration modes. For a single point the turn-around time is always less than the turn-around time when one of the previous methods is used for the study of a general stability problem. For a restrictive study the previous methods might be more efficient than method 2.

   Contrary to previous methods an aeroelastic simulation requires the paradox of utilizing a separate signal analysis procedure to determine frequency and damping information from a microscopic overload of information. This procedure is a parameter identification process in which the aeroelastic model is assumed to be linear and a conventional signal analysis procedure is carried out (e.g. Prony fits, ...), like in the analysis of Ground Vibration Tests or Flight Flutter Tests. Disadvantage is that this procedure only yields results in one point of the flutter diagram (macroscopic underload of information) , and a large number of simulations would be required to obtain sufficient information about the critical flutter boundaries. Also one should try to reduce numerical noise by starting from a well converged flow and geometry or by incorporating well designed low pass filters.

   As an alternative to the conventional curve-fitting procedures a more sophisticated parameter identification process (MIMO) has been developed and applied [HES97, EHS98], which constructs an equivalent linear aeroelastic model having the same properties as the full nonlinear model. This linear model subsequently may be used to obtain complete flutter diagrams in the same way as obtained in conventional flutter analyses, by varying the parameters underlying the identified model, such as dynamic pressure. The combination of this process with aeroelastic simulation reduces the computational effort needed at nonlinear conditions and yields a close complement to conventional methods. The procedure strongly reduces the amount of nonlinear simulations needed, for instance, at transonic flow conditions, where the linear model can be used as a predictor for the critical flutter boundary of the nonlinear system.

   The conventional and the MIMO approach which ’bypasses’ the frequency domain are depicted in figure 1.

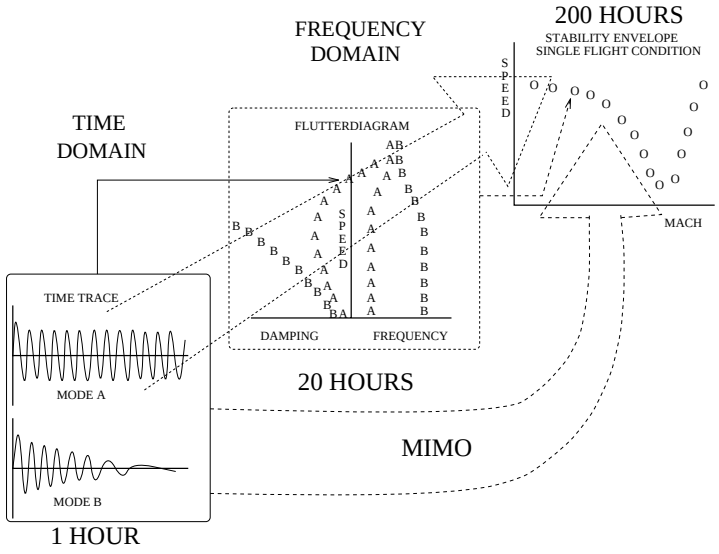

Fig. 1: Conventional and MIMO approach for obtaining flutter points with a coupled time-accurate CFD method.

Experience at NLR has shown that the approach in the k-domain, the s-domain and the time-domain are analogous, as long as the assumption of linearity is not violated and the frequency and time domain methods have no inherent limitations[1] which impair the mapping (fitting of generalized forces) between the separate domains. Also in applying time domain methods for obtaining harmonic data it is important to reduce the level of ambiguity by starting from a well converged *mean* flow or by incorporating low pass filters.

Therefore the fully-coupled simulation may also be performed using a time integration approach of the generalized forces once adequately fitted in the frequency domain. This eases applications (e.g. in case of structural nonlinearities) and improves confidence for the coupled simulation if based on linear aerodynamics.

The two approaches which might be followed to obtain the flutter envelope are depicted in figure 2.

[1] Due to program inconsistencies.

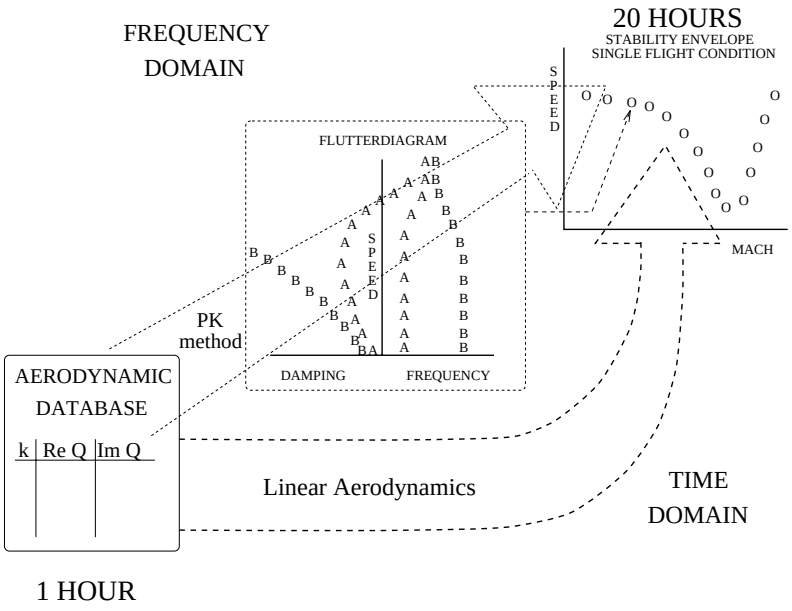

Fig. 2: Frequency domain and time domain approach for obtaining flutter envelopes with a frequency domain method.

Figure 3 show a road map for obtaining time traces with linear aerodynamics. The road map shows the four cornerstones for obtaining generalized forces. The inner blocks denote the applied fitting procedures.

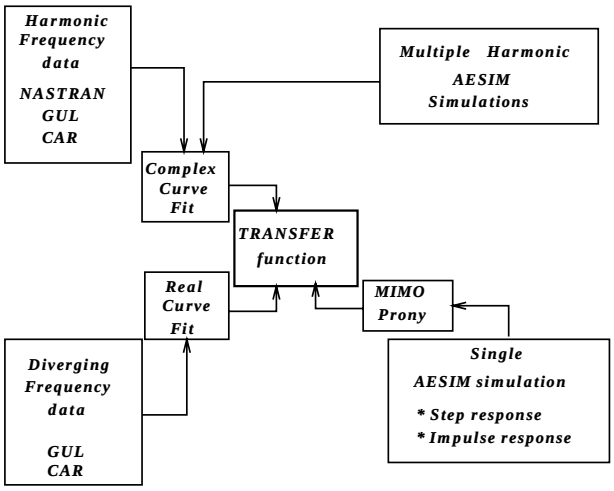

Fig. 3: Road map of tools to transform linear aerodynamics between frequency and time domain.

The successful application of the aforementioned strategies with respect to the AESIM method [HE94] were presented in [HES97, EHS98] where the applications were directed to the AGARD standard aeroelastic test case [Yat88].

Another issue is the dependence of the results on a increased number of parameters (e.g. tolerances) and requirements (e.g. grid quality)[2] which cannot be fully understood nor checked by the aeroelastician and prevents black-box usage. One way to 'solve' the affordability problem might be the employment of coarse grids balanced with 'aeroelastic' accuracy[3].

The aforementioned problems has driven us to find alternative ways for obtaining black-box results from time-accurate CFD (CUA) methods without redesigning them which will be introduced in this report.

In this paper we introduce issues regarding our recent $\frac{[1]\ sample}{cycle}$ and $\frac{[2]\ samples}{cycle}$ concepts for obtaining harmonic and diverging data from time-simulation CFD methods.

The paper presents and discusses preliminary full potential results of applications in unsteady 2-D and 3-D flow.

[2] A prerequisite for a CFD method to be used in an aeroelastic system is a reduced sensitivity to the spacing and principal orientations employed in the grids.

[3] 'aeroelastic' accuracy is defined as the required accuracy for airloads in aeroelastic studies. The type of aeroelastic study being performed sets the accuracy which in many cases is fairly tolerant.

2 Harmonic data from sinusoidal simulation with time-simulation methods

The most common method in obtaining harmonic data is to run a time-domain method in harmonic excitation for a couple of cycles, starting from zero or from a steady state. In general one applies 2-3 cycles and uses the last cycle for deriving the quantities of interest. A periodicity constraint is not applied and there are no reports that the accuracy is monitored during the simulations. When using an impulse or step response the result depends on additional parameters (pulse shape , time-step and observation interval) which endangers a safe use in a black-box environment and requires experimentation. Apart from grid related errors which have been hardly ever assessed from an aeroelastic viewpoint a well designed tolerance criterium to halt inner subiterations is in most cases bypassed by prescribing a fixed (minimal) number for the number of subiterations.

Here we present a different philosophy which can readily be embedded in any CFD method by employing the harmonic constraint $Q - Q^m = A\cos Kt + B\sin Kt$ which approximates a time-linearized approach since we are neglecting the higher harmonics and Q^m is a (mean) steady state solution (potential, density, velocities, energy).

It is described below for a first order method. [1]

Suppose that the airplane performs a sinusoidal motion in one of its modal modes:

$$g = g^m + g^i \sin(Kt),$$

with g the current geometrical state, g^m the mean geometrical state, g^1 a modal mode and K is the frequency of oscillation. Let Q^0, Q^1 and Q^2 denote the current approximation to the solution at $t = 0, \Delta t$ and $2\Delta t$, respectively.

Next, applying the harmonic constraint:

$$Q(t) - Q^m = A\cos(Kt) + B\sin(Kt)$$

and **update**[2] :

[1] We assume that Q^m is not affected by the iteration procedure. When this occurs as a result of a not well converged steady state solution the application of low pass filter techniques for updating Q^m implicitly or to model also Q^m explicitly, which means a $\frac{[3]\ samples}{cycle}$ should be considered.

[2] Higher order temporal schemes will only require the additional update of $Q^{-2}, Q^{\cdot\cdot}$.

$$D = \frac{1}{\cos(\Delta tK)\sin(2\Delta tK) - \cos(2\Delta tK)\sin(\Delta tK)}, \quad (1)$$

$$D1 = (Q^1 - Q^m)\sin(2\Delta tK) - (Q^2 - Q^m)\sin(\Delta tK), \quad (2)$$

$$D2 = \cos(\Delta tK)(Q^2 - Q^m) - \cos(2\Delta tK)(Q^1 - Q^m), \quad (3)$$

$$AC = D1\ D, \quad (4)$$

$$BS = D2\ D, \quad (5)$$

$$Q^0 = Q^m + AC, \quad (6)$$

$$Q^{-1} = Q^m + AC\cos(\Delta tK) - BS\sin(\Delta tK). \quad (7)$$

Then, apply two successive stages of the available time-domain method to improve Q^1 and Q^2.

The harmonic pressures, ..., are directly available:

$$D1 = (cp^1 - cp^m)\sin(2\Delta tK) - (cp^2 - cp^m)\sin(\Delta tK), \quad (8)$$

$$D2 = \cos(\Delta tK)(cp^2 - cp^m) - \cos(2\Delta tK)(cp^1 - cp^m), \quad (9)$$

$$AC = D1\ D, \quad (10)$$

$$BS = D2\ D, \quad (11)$$

$$cp^h = \mathrm{cmplx}(BS, AC). \quad (12)$$

Repeat the whole procedure until the harmonic pressures converges. The flow diagram of the procedure is illustrated in figure 4.

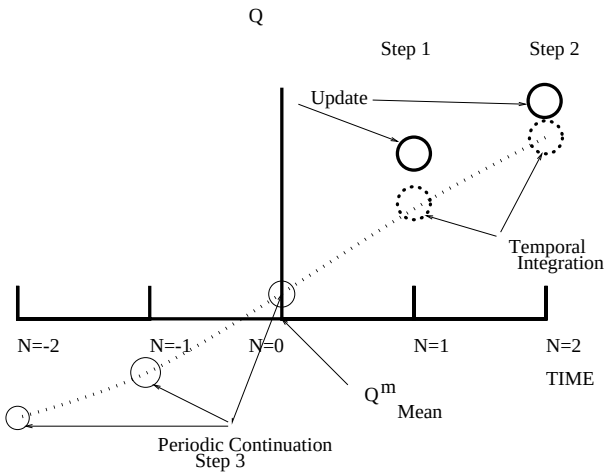

Fig. 4: Temporal flow diagram of the $\frac{[2]\ samples}{cycle}$ concept for sinusoidal motions.

The main advantage of this approach is that it permits a black-box usage since only the time-step and a tolerance for convergence need to be set by the user. By this it approaches the advantage of the linear methods without having to perform the actual linearization.

Our first calculations which update explicitly and are centered about $t = 0$[3] indicate that the procedure has the advantage of being less sensitive to the employed solution methods by enforcing directly the periodicity requirement. It seems to be more robust for larger time steps and faster to convergence. This is probably due to the fact that the calculations are made at the mean position and do not have to cover the extreme positions. More gains might be expected when the solution strategy is tailored to this approach (implicit updating, time-step sequencing, 'multigrid' in time which requires only one additional sample for each level and projection methods [Fis]) and when results are generated by starting from results obtained at neighboring frequencies. It might also be beneficial to use this approach for starting up the common schemes in order to eliminate transients.

A disadvantage is that changes might effect the mean solutions. Also due the applied explicit update convergence will decrease down with decreasing time steps.

[3] It might be expected that anticipating the phase shift, precondition of wake areas and forward prognostication of Q^2 is advantageous.

3 Diverging data from diverging simulation with time-simulation methods

Usage of aeroelastic data for diverging motions seems to be only practiced by NLR and recently by ONERA [Mor97]. This might be explained from the fact that many existing methods do not have the provision for these motions.

Here we present again a different philosophy employing the exponential constraint $Q - Q^m = A\exp(St)$ which approximates a time-linearized approach and is as follows for a first order method:

Suppose that the airplane performs an exponential motion in one of its modal modes:

$$g = g^m + g^i \exp(St),$$

with g the current geometrical state, g^m the mean geometrical state and g^1 a modal mode. Let Q^0 and Q^1 denote the current approximation to the solution at $t = 0$ and Δt,, respectively.

Next, applying the exponential constraint:

$$Q(t) = Q^m + A\exp St,$$

update:

$$Q^{-1} = Q^m + \frac{(Q^1 - Q^m)}{\exp \Delta t S^2}, \tag{13}$$

$$Q^0 = Q^m + \frac{(Q^1 - Q^m)}{\exp \Delta t S}. \tag{14}$$

The diverging rate pressures, ..., are directly available by:

$$cp^d = \frac{(cp^1 - cp^m)}{\exp \Delta t S}. \tag{15}$$

Repeat the whole procedure until the diverging pressures converge. The flow diagram of the procedure is illustrated in figure 5.

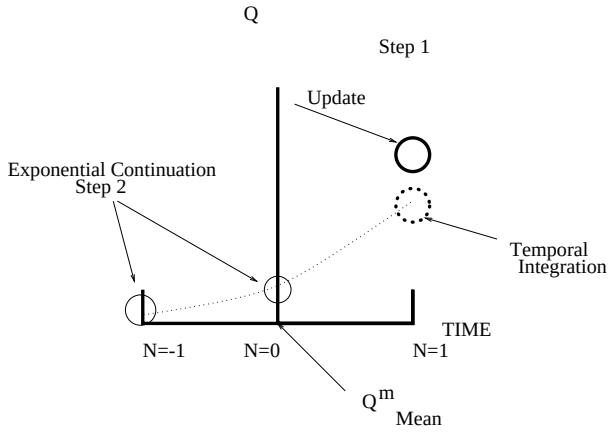

Fig. 5: Temporal flow diagram of the $\frac{[1]\ samples}{cycle}$ concept for diverging rate motions.

Again the main advantage of this approach is that it probably permits a black-box usage since only the time-step and a tolerance for convergence need to be set by the user. By this it approaches the advantage of the linear methods without having to perform the actual linearization. Again the changes might effect the steady state solutions.

4 Aeroelastic Accuracy and Grids

In general we notice that time-accurate CFD applications are made with relatively fine deforming grids and hardly ever we have seen applications on coarse to medium grids which would suit 'aeroelastic' accuracy. The reason seems to be that such applications try to deal with relatively small flow features (leading, trailing edge, shock waves, boundary layer, tip vortices, ..) which might not have that much impact on the 'aeroelastic' results. The other reason is that the principal orientation of applied computational cells are not aligned with the main flow topology. The majority of the flow domain should not be sacrificed for resolving a small flow feature which is not significant to the aeroelastic study..

The application of deforming and adaptable grids might trouble the analysis and simulation as the underlying approaches increase the numerical noise level by adding artificial stiffness, mass and damping and artificial non-linearities (application of limiters to mesh spacing in shock trajectories and near edges) and need constant monitoring of grid quality. For stability problems it is probably safer to apply transpiration conditions.

At NLR a number of methods [Hou89] have been developed which were based on bridging CFD and panel methodology by the so-called Boundary Volume Methodology (BVM). This methodology combines the dimension reduction property of panel methods with a zero mass-flux boundary condition according to a finite difference (volume) full potential method in such a way that only low order accurate aerodynamic potential influence coefficients have to be calculated. The approach requires a computational grid consisting of the body surface and one surface extending above it. This approach has revealed[Hou90] that accurate lift and drag forces can be obtained (thereby recovering D'Alembert's paradox) for the flow around a flat plate up to 90 deg angle of attack using a **full**[1] chord spacing along the plate and half a chord spacing in normal direction!

Therefore it is fair to expect that subcritical subsonic flows and supersonic flows can be modeled with coarse to medium fine grids provided that in a large domain of the flow the computational cells are well aligned with the main flow direction. The latter is the reason that the AESIM method primarily applies a HO main grid for resolving the main flow features. It has also be noted in [FNW97] that flutter results are very sensitive to the topology of the applied grid. The applications shown in this paper are mainly applied on coarse to medium grids to illustrate that results with 'aeroelastic' accuracy can be obtained on these grids.

[1] One computational cell.

5 Recent AESIM developments

Apart from the integration of the aforementioned temporal schemes recently attention was given to support dynamic loads studies.

5.1 Dynamic loads and sectional forces

Time traces of dynamic loads have to be calculated and analyzed for parts and sections of the aircraft. The latter involves the arbitrary cutting of components and the calculation of dynamic traces of the elastomechanical forces and aerodynamic forces on specific parts. The AESIM method performs these activities on the basis of bounding boxes to be specified by the user of which the starboard face performs the cutting. The sectional pressure coefficients are obtained by interpolating with a 6-NNB Laplace type volume spline which employs a core-regularization borrowed from the discrete auto influence calculation of field panels influence coefficients as reported in [Hou85]. Sectional loads coefficients are obtained by integrating the interpolated pressures along the interpolated contours.

5.2 Arbitrary gust field specification

To support general dynamic loads applications the induced velocity field of a gust is written as:

$$\vec{W}_g^i = q_a^i \vec{G}^i \tau_x^i \tau_y^i \tau_z^i, \tag{16}$$

where q_a^i is the amplitude of the gust mode i and $\vec{G}$ denotes the directional components. The gust mode is factored in three directions to enable a general application:

$$\tau_x = \left\{ \; (1+U_g)(\tau(x_e - x_{\text{off}} - (U_\infty - U_g)t)) \qquad , \right. \tag{17}$$

$$\tau_y = \left\{ \; (1+V_g)(\tau(y_e - y_{\text{off}} - (V_\infty - V_g)t)) \qquad , \right. \tag{18}$$

$$\tau_z = \left\{ \; (1+W_g)(\tau(z_e - z_{\text{off}} - (W_\infty - W_g)t)) \qquad . \right. \tag{19}$$

U_g, V_g, W_g denote the relative velocity components of the gust, x_e, y_e, z_e are the coordinates of the aerodynamic grid, $x_{\text{off}}, y_{\text{off}}, z_{\text{off}}$ are the offsets which might be used to activate the gust at the right time, and $U_\infty, V_\infty, W_\infty$, denote the velocity of the aircraft. The functions τ are user selectable.

6 Applications

The examples here focus mainly on current ongoing activities with respect to the new temporal schemes. Especially attention is given to the modeling of a flat plate at a relatively low Mach number using the full potential model. The latter model is more sensitive to the temporal integration schemes as compared to Euler models.

6.1 Two-dimensional flat plate application

Calculations of unsteady airloads have been performed with AESIM using the full potential modeling for a flat plate pitching about 25% chord ,$M_\infty = 0.5$ and a reduced frequency range up to $\mid s \mid = 1.6$. [1] The amplitude is 0.25 deg. The generalized forces data are compared to DOULAT data generated with 100 panels. Two subiteration procedures to integrate within a time step have been used:

S2U Standard 2-Newton subiterations using one AF3 sweep.

H5U Robust 5-Newton subiterations using one AF3 sweep, local time stepping and GMRES[SS86] with AF3 preconditioning and up to 8 Krylov vectors.

The first scheme is the one most common applied. The second one aims at reducing the error strongly in a time step to allow for coarse time steps.

The H topology grids used in the AESIM simulations are depicted in figures 6..9. Figure 6 shows the overall fine grid and figure 7 shows a close-up near the plate. Figure 8 shows the coarse grid obtained after reducing the fine grid with about a factor 4 and again figure 9 shows a close-up near the plate.

The results consist of:

Figures 10..15 Coarse grid simulation using 3 cycles with 12 time steps per cycle ($\frac{CYCLE}{12}$) at k=0.1 with S2U updating. In figures 10 and 13 the development of the forces for the regular scheme and the 2-sample scheme are presented. It should be noted that the latter result show only the development of the two samples!. Both results are not converged due to a large CFL number (400). Convergence characteristics are shown in figures 11 and 12 for the regular scheme. LEUCR and LEUCC denote the L_2 norm of the error in the equations and the corrections, respectively. LINFR and LINFC denote the L_∞ norm of the error in the equations and the corrections, respectively.

Note the latter figure applies a log scale to the results which are also shown in the first figure. The unscaled figures should be preferred in assessing convergence during time simulation as

[1] The reduced frequency is defined here as $k = Im(s) = \frac{\omega c}{2U}$ where c denotes the chord.

the log scale filter might hide information. Convergence characteristics are shown in figures 14 and 15 for the 2-sample scheme.

Figures 16..21 Coarse grid simulation using 3 cycles with 12 time steps per cycle ($\frac{CYCLE}{12}$) at k=0.1 with H5U updating. In figures 16 and 19 the development of the forces for the regular scheme and the 2-sample scheme are presented. Again it should be noted that the latter result show only the development of the two samples!. Both results seem to be converged. Convergence characteristics are shown in figures 17 and 18 for the regular scheme. Again note the latter figure applies a log scale to the results which are also shown in the first figure. The convergence characteristics which are shown in figures 20 and 21 for the 2-sample scheme seem to be better.

Figures 22..27 Coarse grid simulation using 3 cycles with 12 time steps per cycle ($\frac{CYCLE}{12}$) at k=1.0 with H5U updating. In figures 22 and 25 the development of the forces for the regular scheme and the 2-sample scheme are presented. Both results seem to be converged. Convergence characteristics are shown in figures 23 and 24 for the regular scheme. The convergence at the higher frequency is better as compared to the one obtained for the lower frequency. The convergence characteristics which are shown in figures 26 and 27 for the 2-sample scheme seem to be better. The convergence at the lower frequency is better as compared to the one obtained for the higher frequency.

Figures 28..35 Fine grid simulation using 3 cycles with 12 time steps per cycle ($\frac{CYCLE}{12}$) at k=0.1 with H5U updating. In figures 28 and 31 the development of the forces for the regular scheme and the 2-sample scheme are presented. Again it should be noted that the latter result show only the development of the two samples!. The regular scheme results on the fine grid do not convergence while the 2-sample scheme converges. The regular scheme is not converged due to the fact that the CFL number which approaches 2000 is too high. The time-step and/or the number of subiterations need to be increased to get a proper result. The Convergence characteristics are shown in figures 29 and 30 for the regular scheme. Inspection of the convergence levels in this case (figure 30) leads to the conclusion that it is hard to base the quality of the prediction on these figures! The convergence characteristics which are shown in figures 32 and 33 for the 2-sample scheme seem to be better. In figures 34 and 34 the pressure distributions for the regular scheme and the 2-sample scheme are presented. The 2-sample scheme results seem to be all right. The regulars scheme results are wrong. They seem to lag 90 deg in phase. The 2-sample approach seems to be more tolerant to the solver.

Figure 36 Convergence study with respect to the sectional forces of the 2-sample scheme versus number of iterations on the coarse grid at k=0.1 with 2-sample scheme and H5U updating (note the scales). In this case the time step was chosen fixed to $\frac{CYCLE}{12}$ and the number

of cycles was varied (1,2,4,8 and 16 cycles). About 20 iterations seem to be necessary for obtaining adequate results.

Figure 37 Convergence study with respect to the sectional forces of the 2-sample scheme versus number of iterations on the coarse grid at k=0.1 with two sample scheme and S2U updating (note the scales). In this case the time step was chosen fixed to $\frac{CYCLE}{12}$ and the number of cycles was varied (1,2,4,8 and 16 cycles). About 300 iterations seem to be necessary for having adequate results.

Figure 38 Convergence study with respect to the sectional forces of the 2-sample scheme versus time step on the coarse grid at k=0.1 with 2-sample scheme and H5U updating (note the scales). Two types of results are depicted. The first set fixes the number of cycles to 3 and the number of time steps per cycle varies ($\frac{CYCLE}{2,4,8,16,32\text{and}48}$). The second set is run with a sufficient number of cycles to obtain converged data. The imaginary part seem to be much dependent on the time-step. The results demonstrate that starting at 12 time steps per cycle adequate result might be obtained. A disadvantage due to the explicit nature of the current 2-sample scheme implementation is that 3 cycles are no longer sufficient at smaller time steps. The latter problem might be easily cured by coarse to fine time-step sequencing.

Figure 39 A comparison between several methods. The figure shows results of DOULAT, results of the 2-sample scheme and the regular scheme on both the fine and the coarse grid. The CFD results were generated with the afore mentioned strategy. The following observations can be made[2]:

- The DOULAT results compare reasonably well with both CFD results on the coarse grid over the entire frequency range, except for the real part of the moment coefficient.
- The CFD results on the fine grids reveal that the 2-sample scheme is the better choice when a coarse time-stepping is applied. At the lower frequencies the regular scheme is too much effected by convergence problems.
- The 2-sample scheme requires a time step of $\frac{CYCLE}{24}$ for an adequate accuracy over the frequency domain.
- The CFD results on the fine grids reveal that the regular scheme is the better choice when a fine time-stepping is applied. At the higher frequencies the 2-sample scheme is too much effected by the current explicit implementation.

Figures 40..42 Fine grid diverging simulation using 3 x 12 time steps at k=0.1 with H5U updating. Nice convergence characteristics are shown in figures 40 and 41 for the 1-sample scheme. 42 shows the pressure distributions for the 1-sample scheme which seem to be all right.

[2] One should hold in mind that the CFD methods solve the full potential equation on a finite domain while DOULAT solves the Prandl-Glauert equation on an infinite domain.

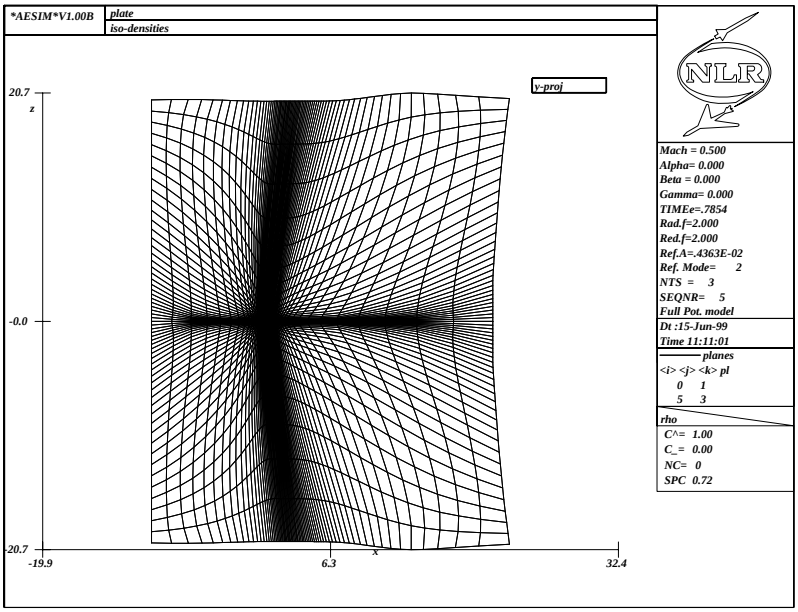

Fig. 6: Fine H grid around flat plate.

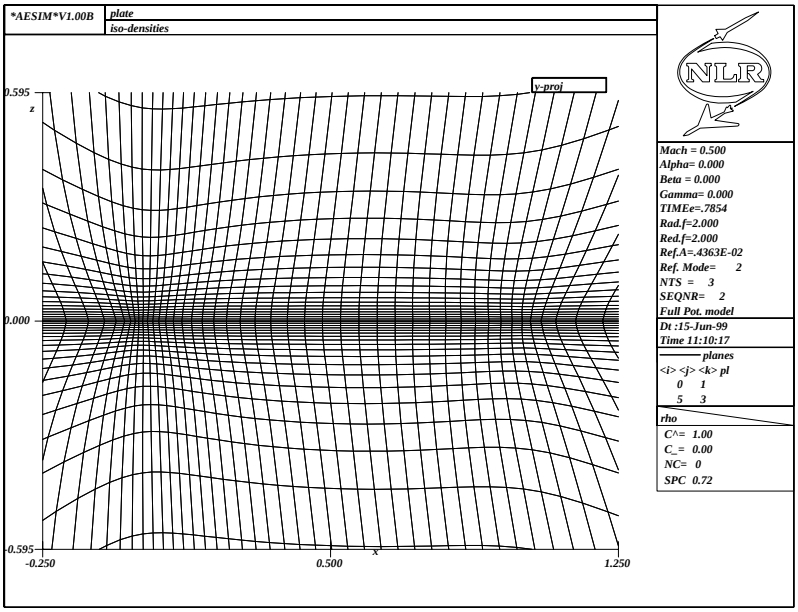

Fig. 7: Fine H grid around flat plate (close-up).

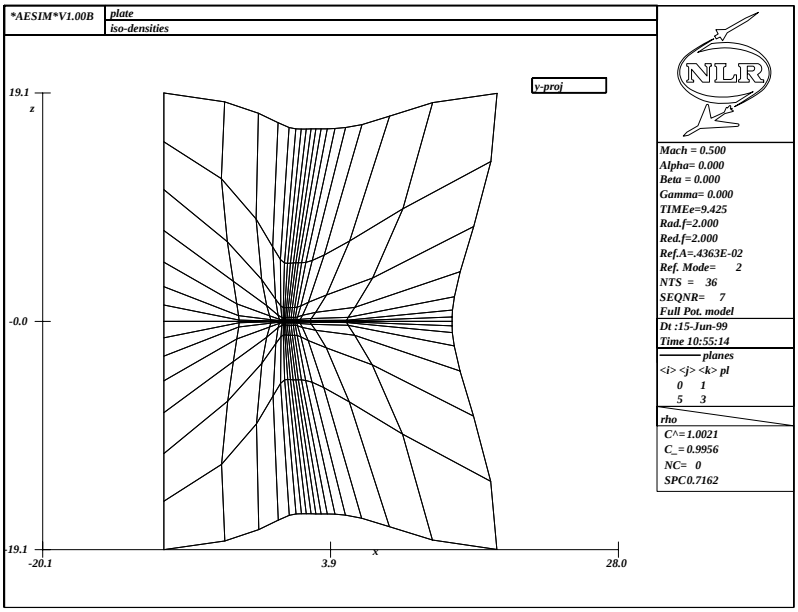

Fig. 8: Coarse H grid around flat plate.

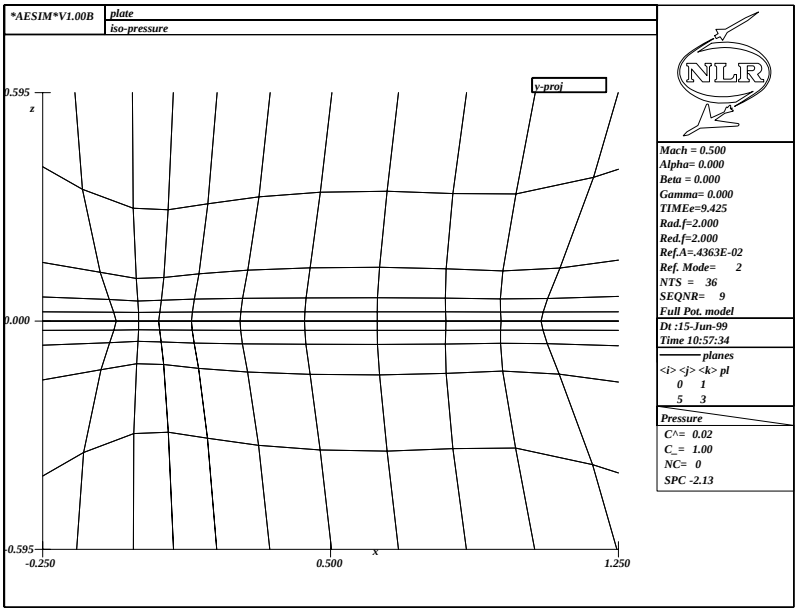

Fig. 9: Coarse H grid around flat plate (close-up).

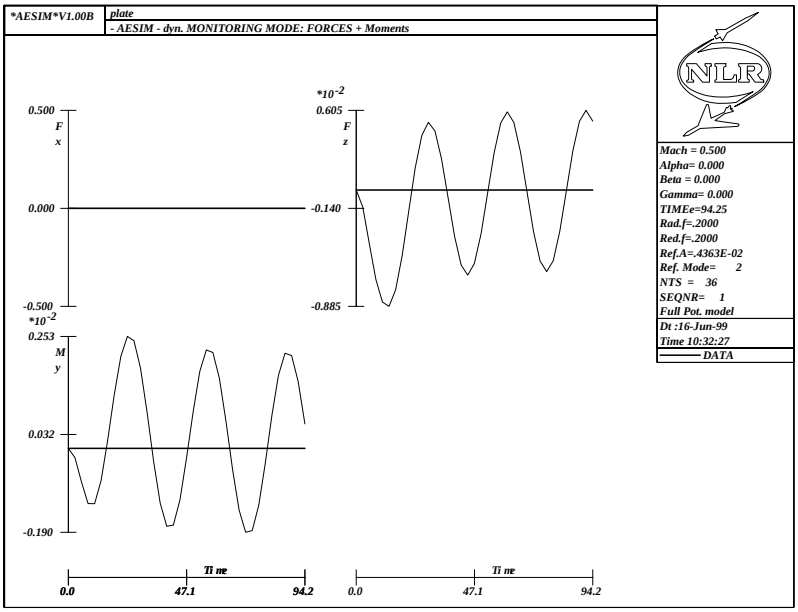

Fig. 10: Dynamic forces on flat plate at $M_\infty = 0.5$ and $k = 0.1$ on the coarse grid with S2U updating.

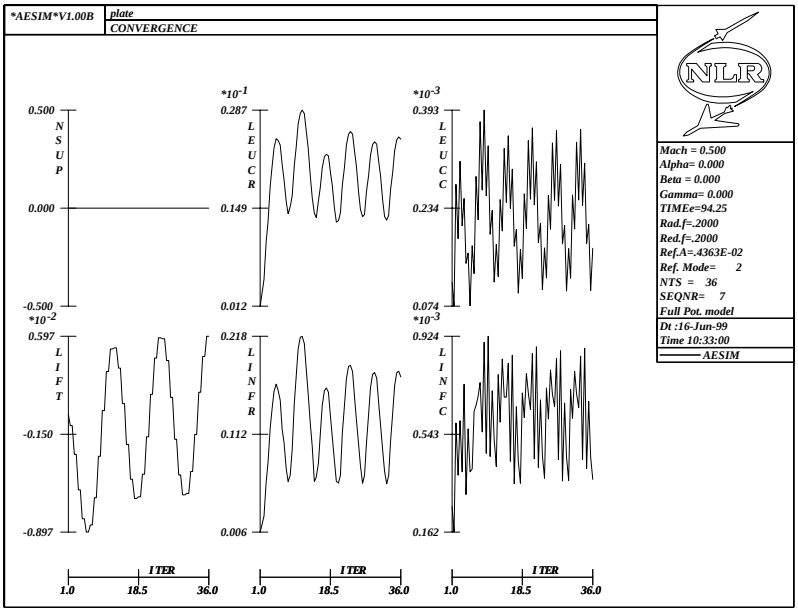

Fig. 11: Convergence characteristics during dynamic simulation on flat plate at $M_\infty = 0.5$ and $k = 0.1$ on the coarse grid with S2U updating.

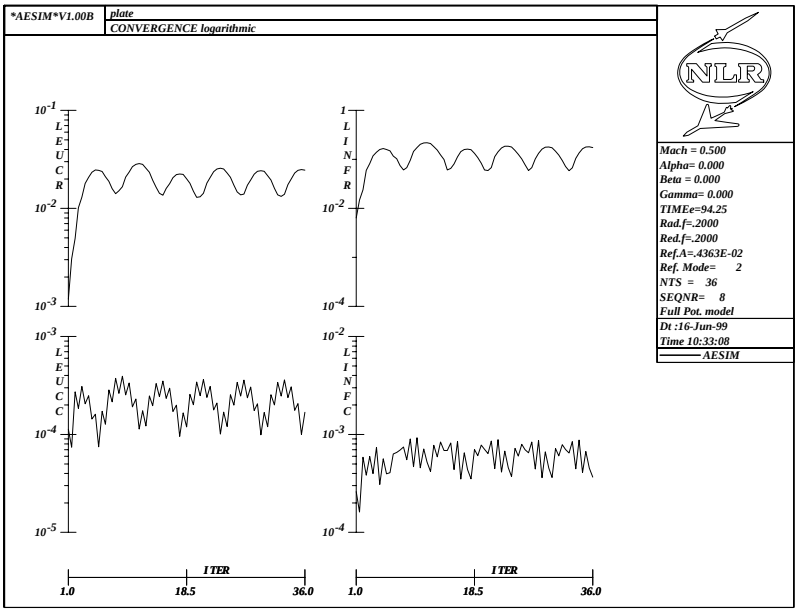

Fig. 12: Convergence characteristics during dynamic simulation on flat plate (log scale) at $M_\infty = 0.5$ and $k = 0.1$ on the coarse grid with S2U updating.

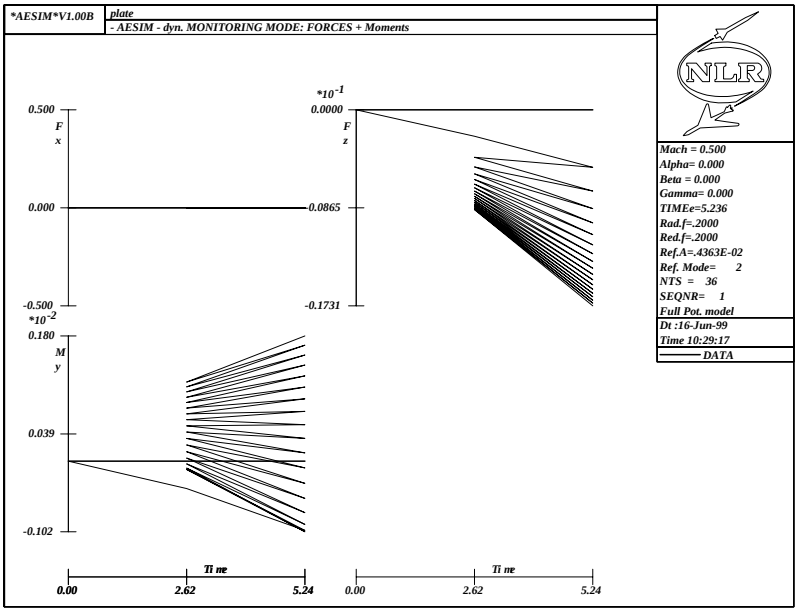

Fig. 13: Convergence of dynamic forces on flat plate with the 2-sample scheme at $M_\infty = 0.5$ and $k = 0.1$ on the coarse grid with S2U updating.

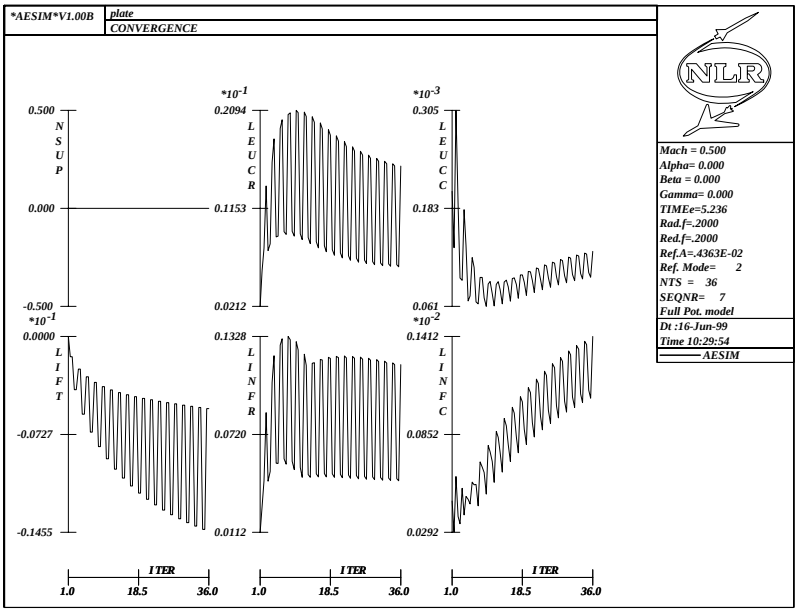

Fig. 14: Convergence characteristics during dynamic simulation on flat plate with the 2-sample scheme at $M_\infty = 0.5$ and $k = 0.1$ on the coarse grid with S2U updating.

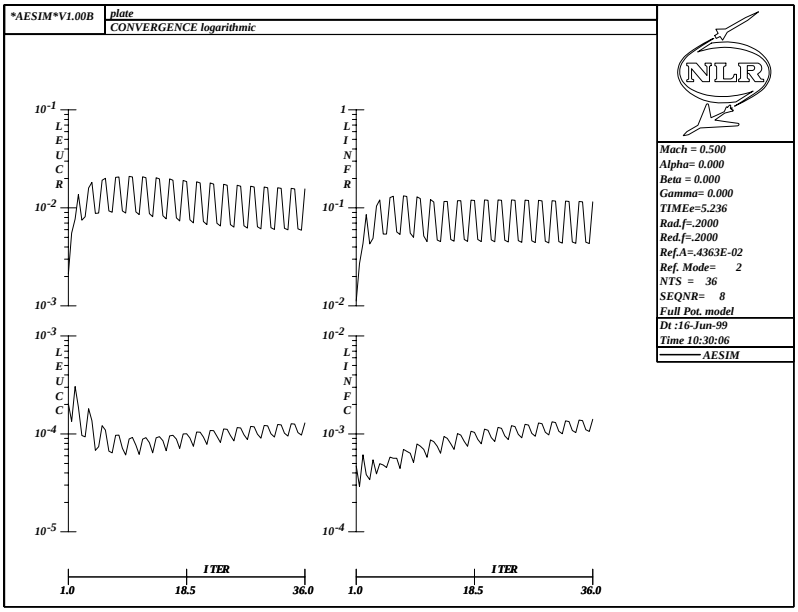

Fig. 15: Convergence characteristics during dynamic simulation on flat plate (log scale) with the 2-sample scheme at $M_\infty = 0.5$ and $k = 0.1$ on the coarse grid with S2U updating.

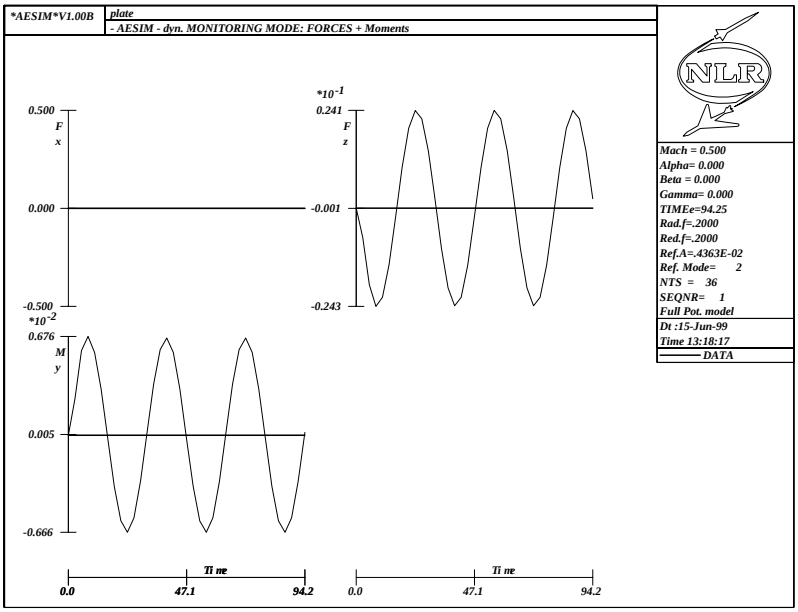

Fig. 16: Dynamic forces on flat plate at $M_\infty = 0.5$ and $k = 0.1$ on the coarse grid with H5U updating.

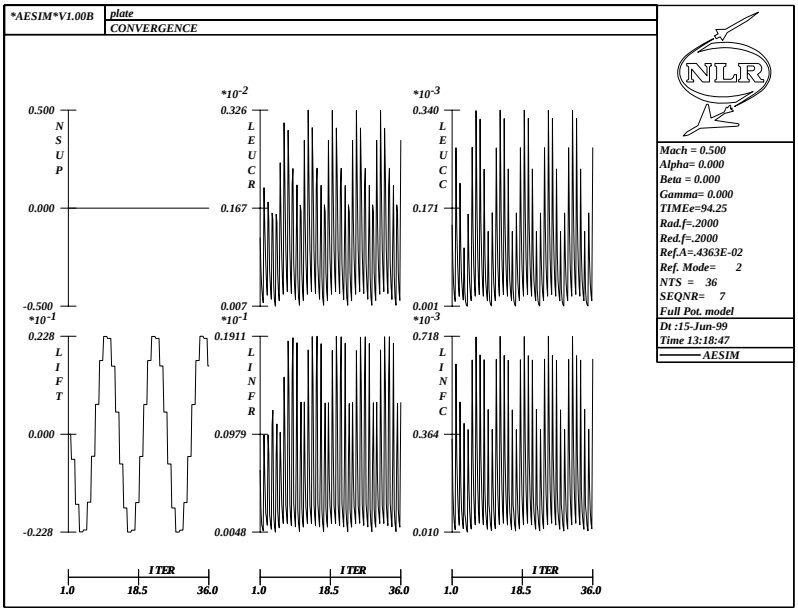

Fig. 17: Convergence characteristics during dynamic simulation on flat plate at $M_\infty = 0.5$ and $k = 0.1$ on the coarse grid with H5U updating.

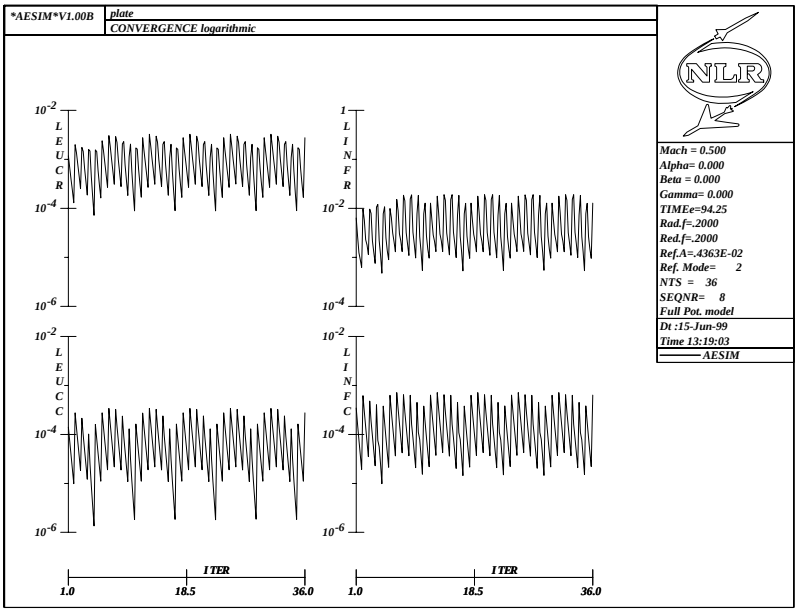

Fig. 18: Convergence characteristics during dynamic simulation on flat plate (log scale) at $M_\infty = 0.5$ and $k = 0.1$ on the coarse grid with H5U updating.

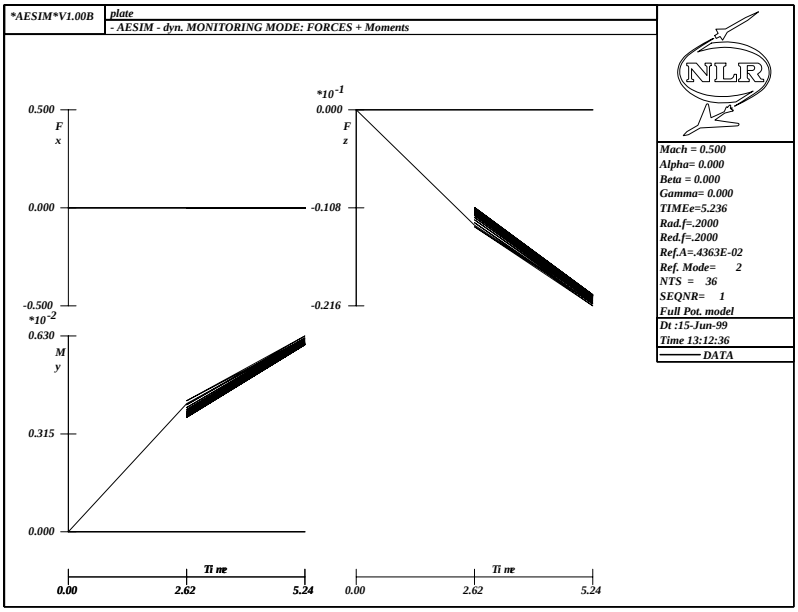

Fig. 19: Convergence of dynamic forces on flat plate with the 2-sample scheme at $M_\infty = 0.5$ and $k = 0.1$ on the coarse grid with H5U updating.

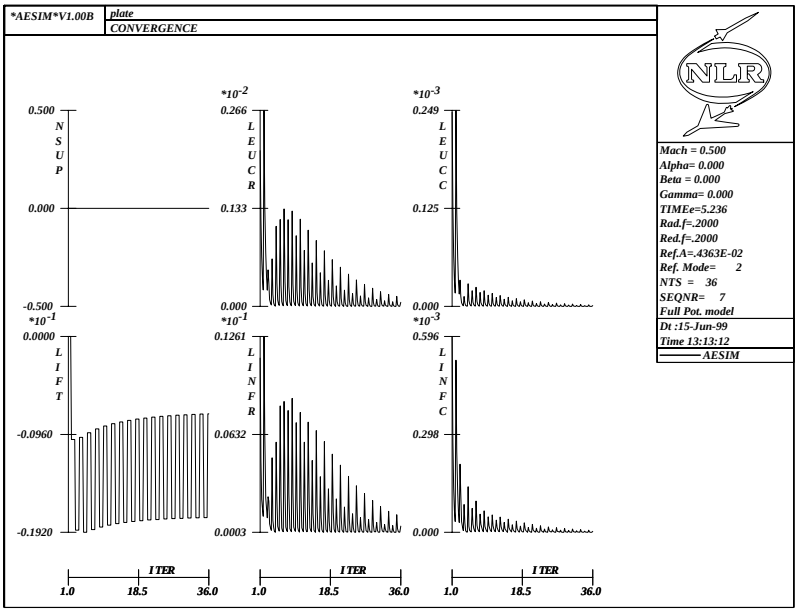

Fig. 20: Convergence characteristics during dynamic simulation on flat plate with the 2-sample scheme at $M_\infty = 0.5$ and $k = 0.1$ on the coarse grid with H5U updating.

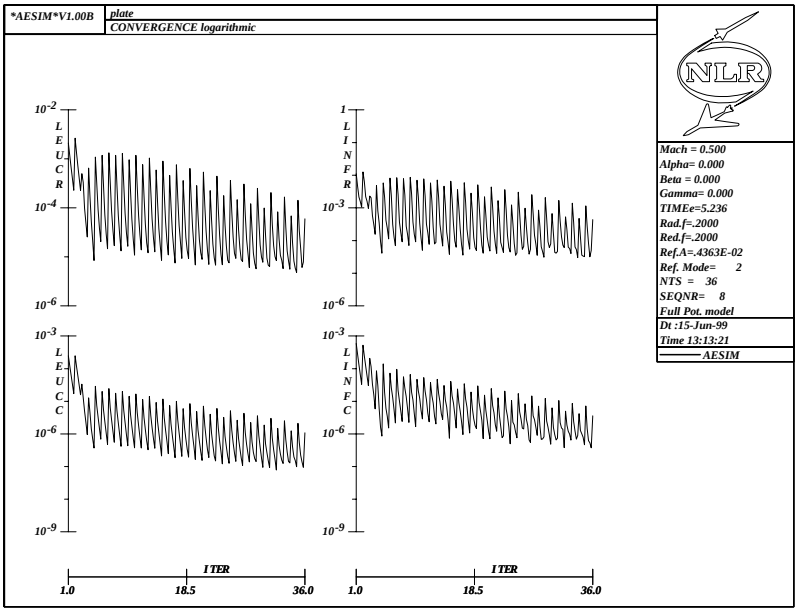

Fig. 21: Convergence characteristics during dynamic simulation on flat plate (log scale) with the 2-sample scheme at $M_\infty = 0.5$ and $k = 0.1$ on the coarse grid with H5U updating .

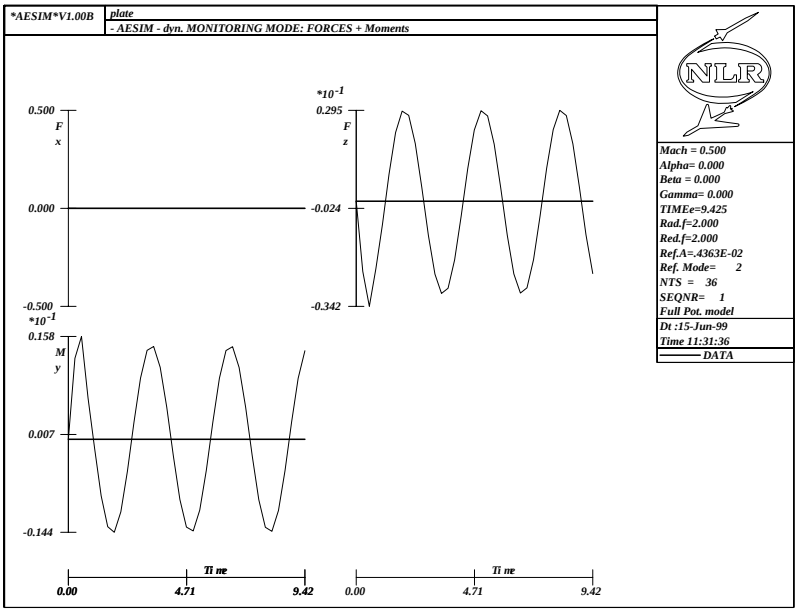

Fig. 22: Dynamic forces on flat plate at $M_\infty = 0.5$ and $k = 1.0$ on the coarse grid with H5U updating.

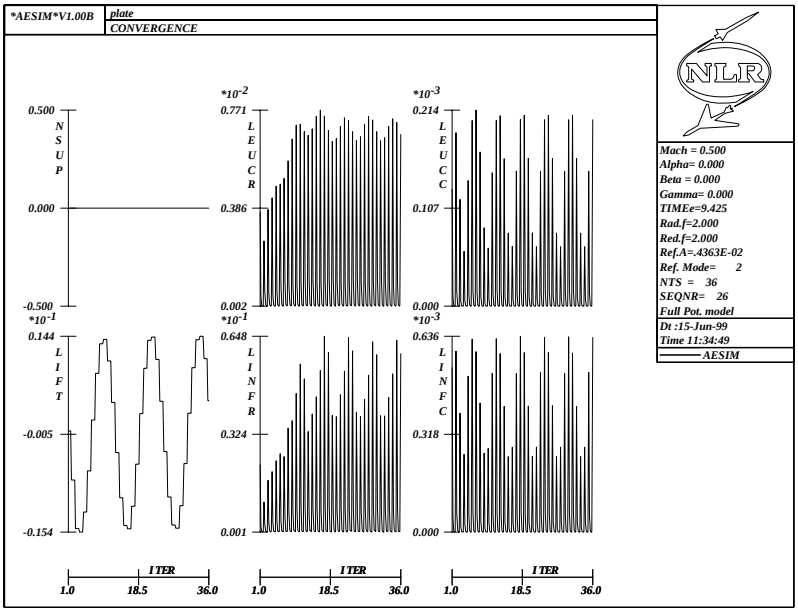

Fig. 23: Convergence characteristics during dynamic simulation on flat plate at $M_\infty = 0.5$ and $k = 1.0$ on the coarse grid with H5U updating.

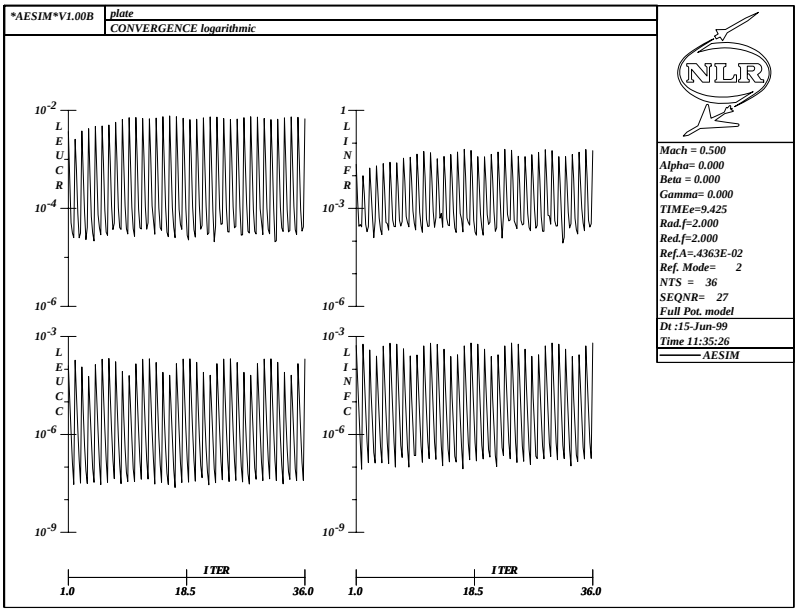

Fig. 24: Convergence characteristics during dynamic simulation on flat plate (log scale) at $M_\infty = 0.5$ and $k = 1.0$ on the coarse grid with H5U updating.

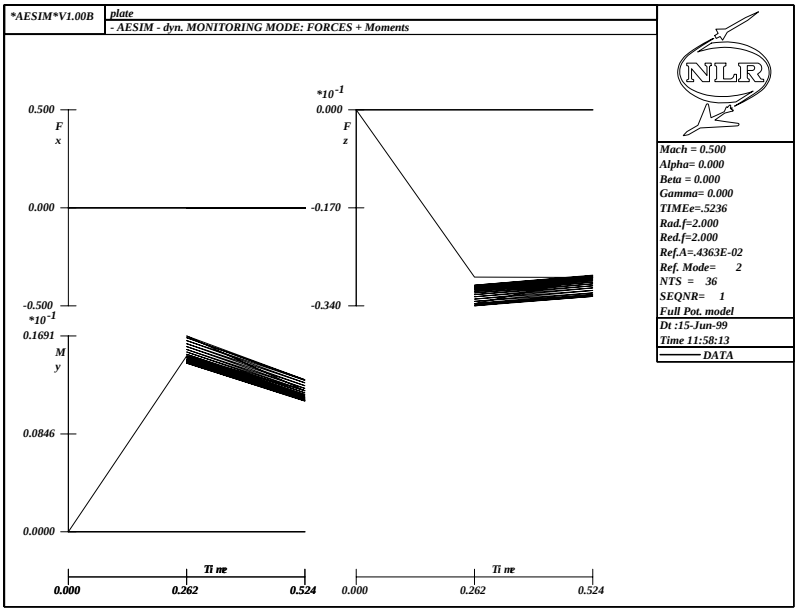

Fig. 25: Convergence of dynamic forces on flat plate with the 2-sample scheme at $M_\infty = 0.5$ and $k = 1.0$ on the coarse grid with H5U updating.

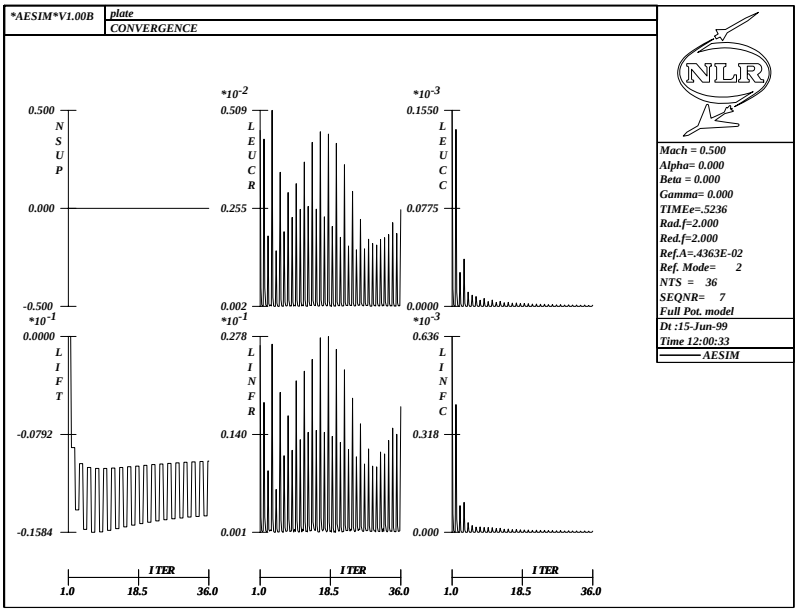

Fig. 26: Convergence characteristics during dynamic simulation on flat plate with the 2-sample scheme at $M_\infty = 0.5$ and $k = 1.0$ on the coarse grid with H5U updating .

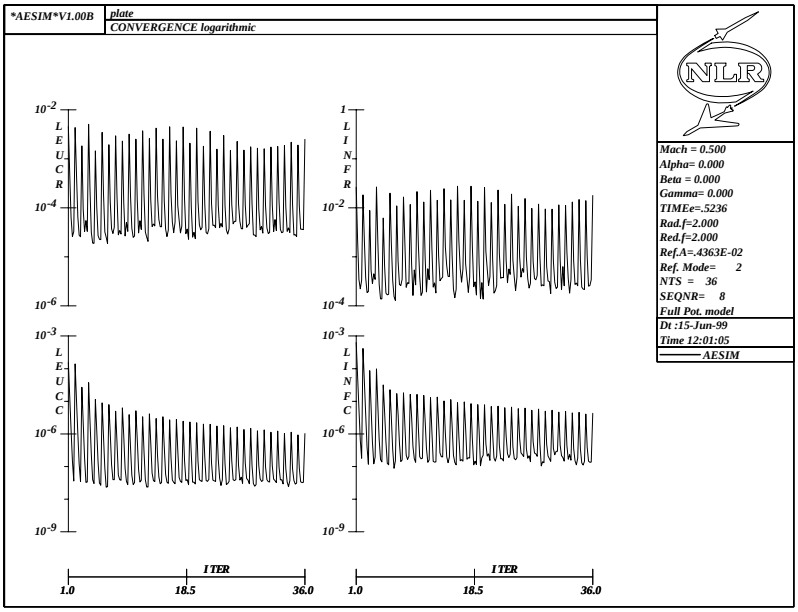

Fig. 27: Convergence characteristics during dynamic simulation on flat plate (log scale) with the 2-sample scheme at $M_\infty = 0.5$ and $k = 1.0$ on the coarse grid with H5U updating.

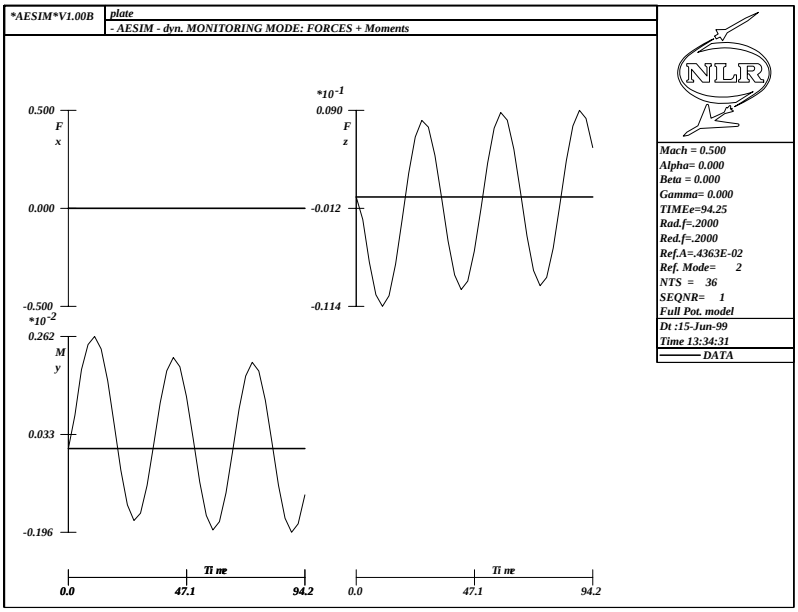

Fig. 28: Dynamic forces on flat plate at $M_\infty = 0.5$ and $k = 0.1$ on the fine grid with H5U updating.

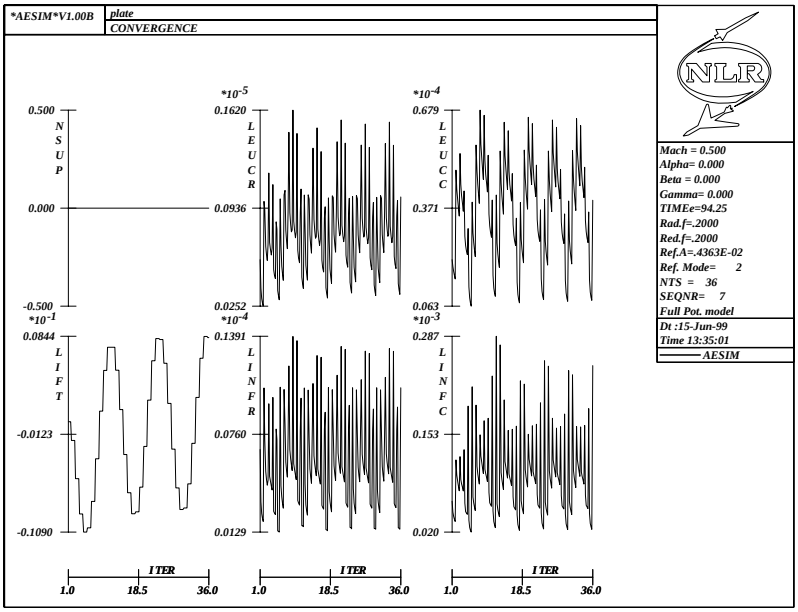

Fig. 29: Convergence characteristics during dynamic simulation on flat plate at $M_\infty = 0.5$ and $k = 0.1$ on the fine grid with H5U updating.

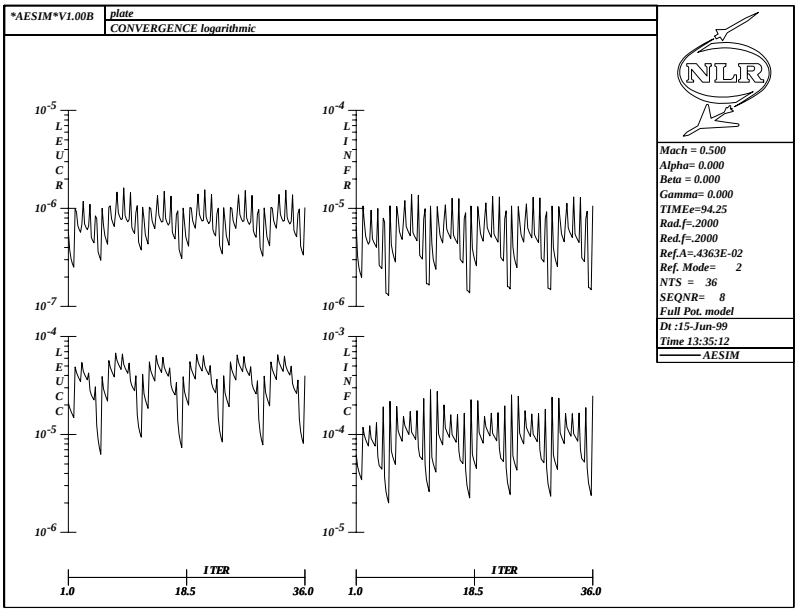

Fig. 30: Convergence characteristics during dynamic simulation on flat plate (log scale) at $M_\infty = 0.5$ and $k = 0.1$ on the fine grid with H5U updating.

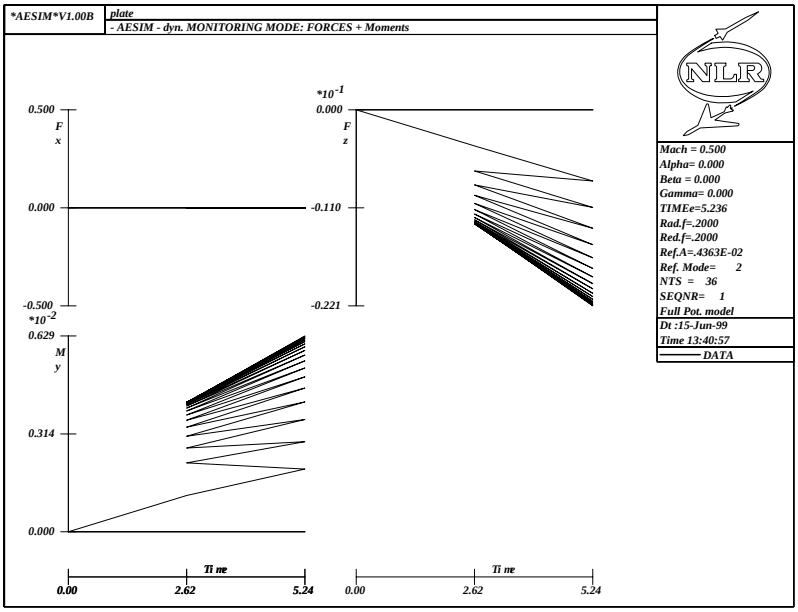

Fig. 31: Convergence of dynamic forces on flat plate with the 2-sample scheme at $M_\infty = 0.5$ and $k = 0.1$ on the fine grid with H5U updating.

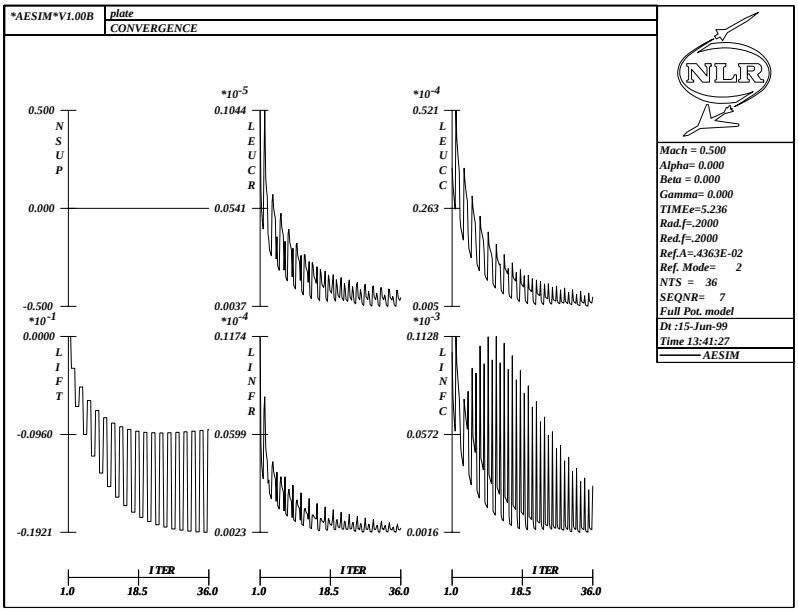

Fig. 32: Convergence characteristics during dynamic simulation on flat plate with the 2-sample scheme at $M_\infty = 0.5$ and $k = 0.1$ on the fine grid with H5U updating.

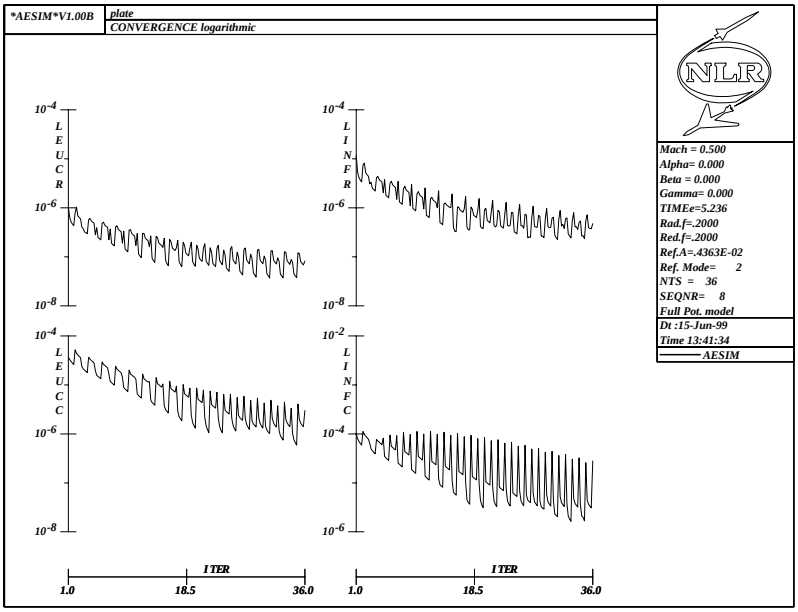

Fig. 33: Convergence characteristics during dynamic simulation on flat plate (log scale) with the 2-sample scheme at $M_\infty = 0.5$ and $k = 0.1$ on the fine grid with H5U updating.

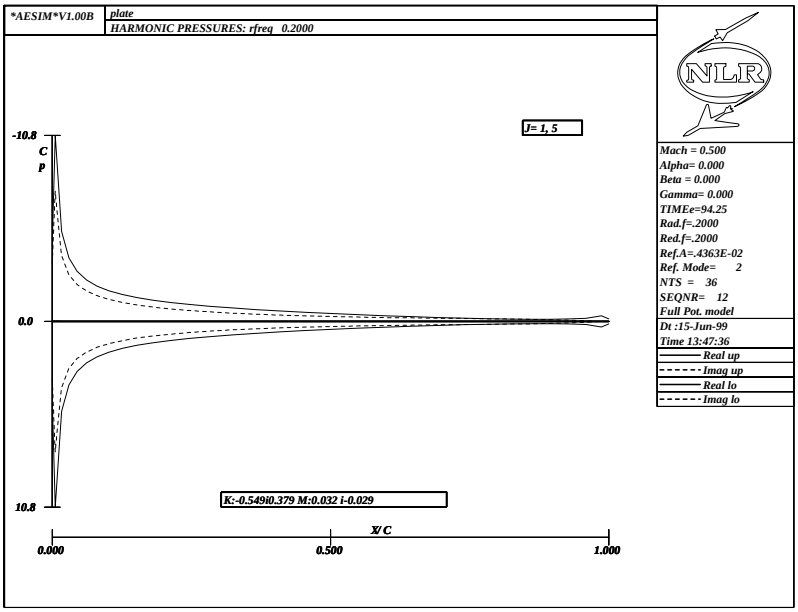

Fig. 34: **Non** converged harmonic pressure coefficient distributions on flat plate at $M_\infty = 0.5$ and $k = 0.1$ on the fine grid with H5U updating.

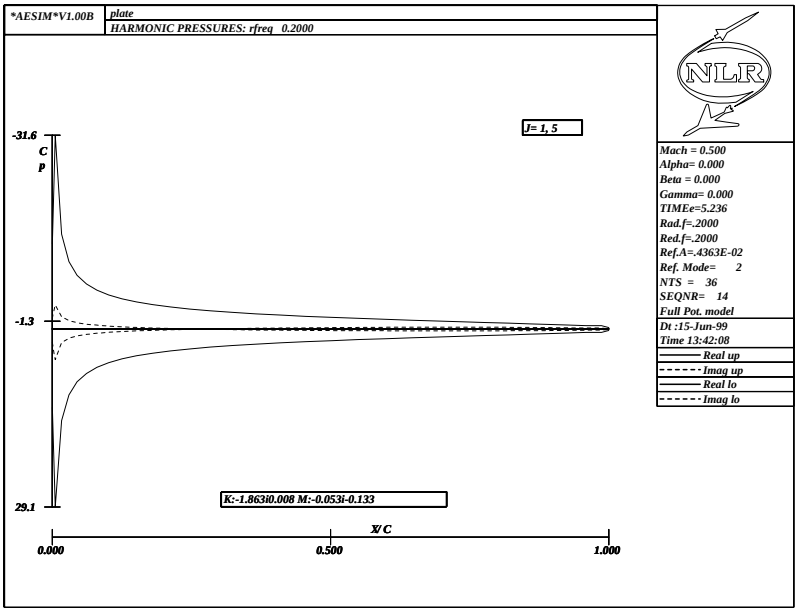

Fig. 35: Harmonic pressure coefficient distributions on flat plate with the 2-sample scheme at $M_\infty = 0.5$ and $k = 0.1$ on the fine grid with H5U updating.

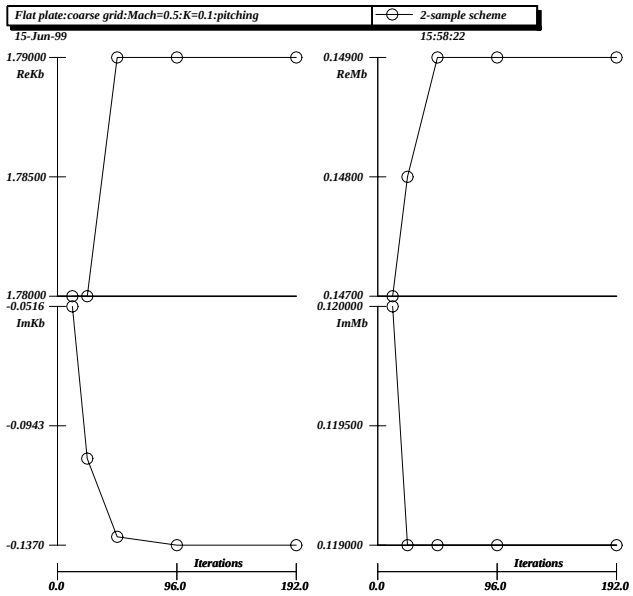

Fig. 36: Convergence of sectional forces of 2-sample scheme versus number of iterations on flat plate at $M_\infty = 0.5$ and $k = 0.1$ on the coarse grid with H5U updating.

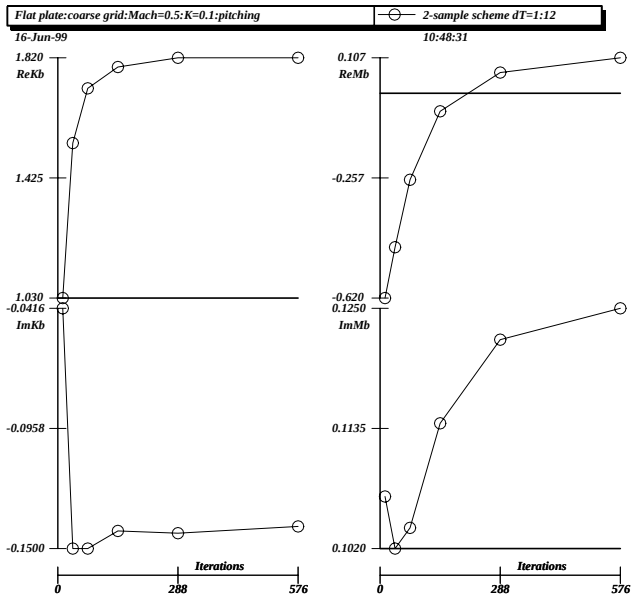

Fig. 37: Convergence of sectional forces of 2-sample scheme versus number of iterations on flat plate at $M_\infty = 0.5$ and $k = 0.1$ on the coarse grid with S2U updating.

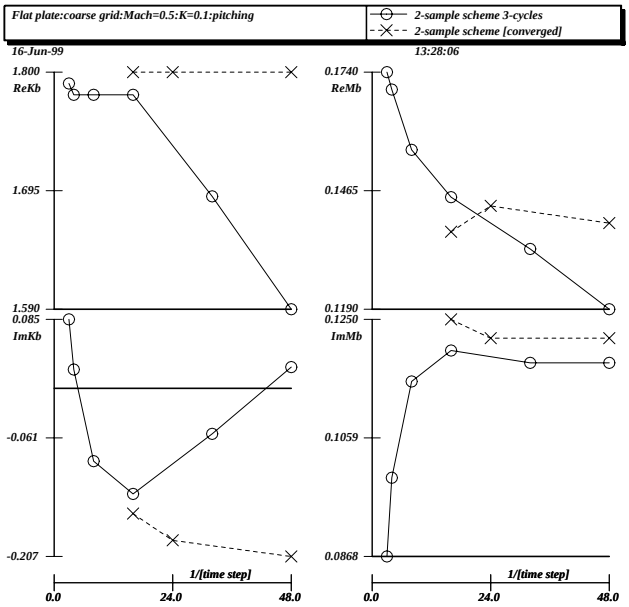

Fig. 38: Convergence of 2-sample scheme versus time step on flat plate at $M_\infty = 0.5$ and $k = 0.1$ on the coarse grid with H5U updating.

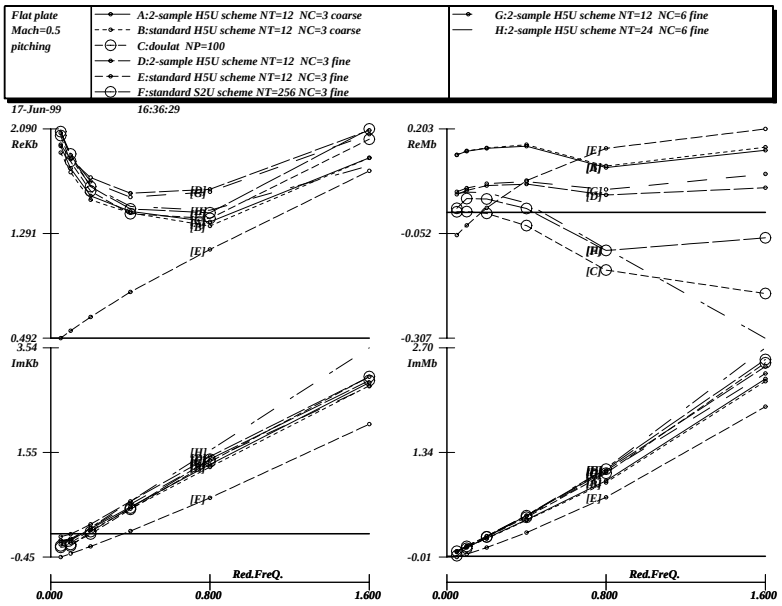

Fig. 39: Comparison of lift and moment coefficients on pitching flat plate at $M_\infty = 0.5$.

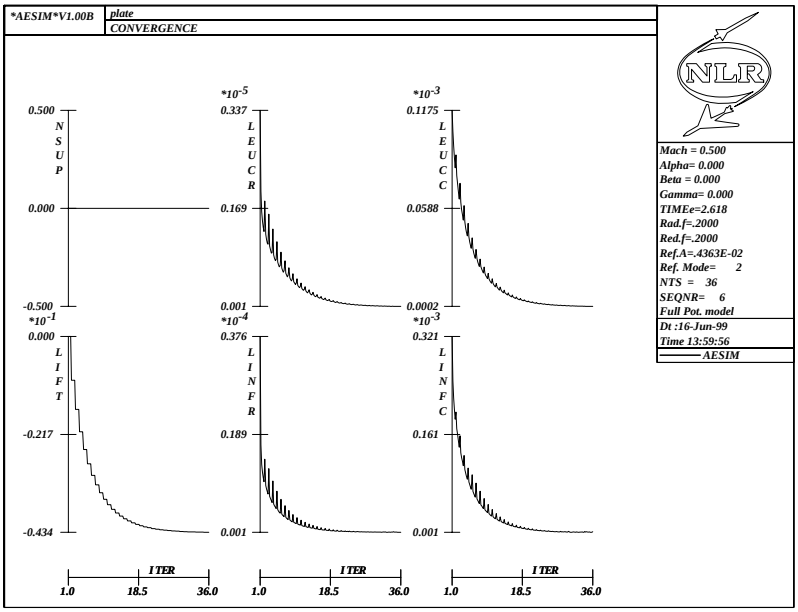

Fig. 40: Convergence characteristics during dynamic diverging rate simulation on flat plate with the 1-sample scheme at $M_\infty = 0.5$ and $k = 0.1$ on the fine grid with H5U updating.

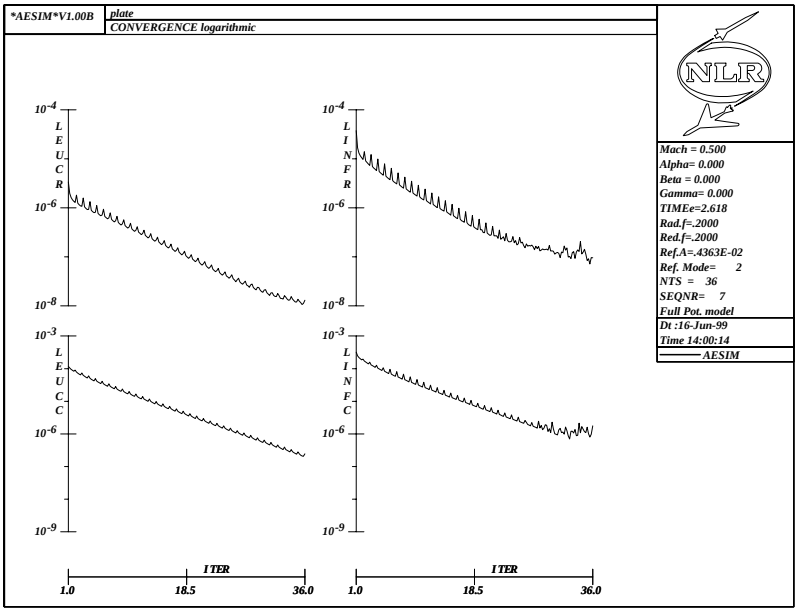

Fig. 41: Convergence characteristics during dynamic diverging rate simulation on flat plate with the 1-sample scheme (log scale) at $M_\infty = 0.5$ and $k = 0.1$ on the fine grid with H5U updating.

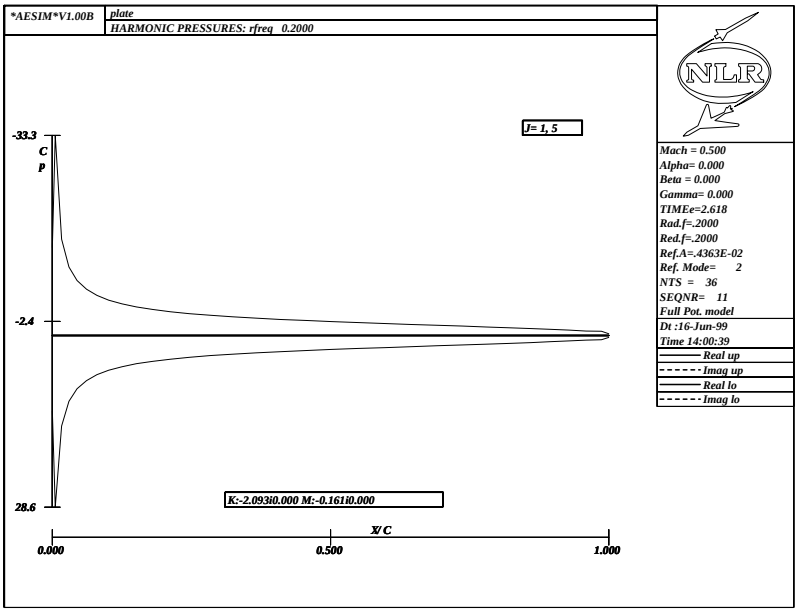

Fig. 42: Diverging rate pressure distributions on flat plate obtained with the 1-sample scheme (log scale) at $M_\infty = 0.5$ and $k = 0.1$ on the fine grid with H5U updating.

6.2 Two-dimensional NACA 64A010 application

To demonstrate the applicability of the 2-sample scheme for a transonic case the NACA64A010 airfoil has been selected.

Calculations of unsteady airloads have been performed with AESIM using the full potential modeling for the NACA 64A010 airfoil at $M_\infty = 0.8$ and a reduced frequency range up to $\mid s \mid = 0.8$. The oscillation was a 0.5 deg pitching about 25% chord. The H5U and the 2-sample scheme was selected applying 72 iterations with the time step equivalent to$\frac{CYCLE}{18}$.

The results consist of:

Figures 43..46 Fine grid simulation using 4 cycles with 18 time steps per cycle at k=0.2 with H5U updating. In figure 43 the development of the forces for the 2-sample scheme is presented. It should be noted that the latter result show only the development of the two samples!. Convergence characteristics are shown in figures 44 and 45. In figure 46 the pressure distributions for the 2-sample scheme are presented which seems to be all right.

Figure 47 A comparison between several methods is shown in figure 47. The figure shows results of DOULAT, results of the 2-sample scheme up to k=0.4[3] and results of the regular scheme up to k=1.0. The agreement between the CFD results is fairly good. The imaginary part seems to be most sensitive.

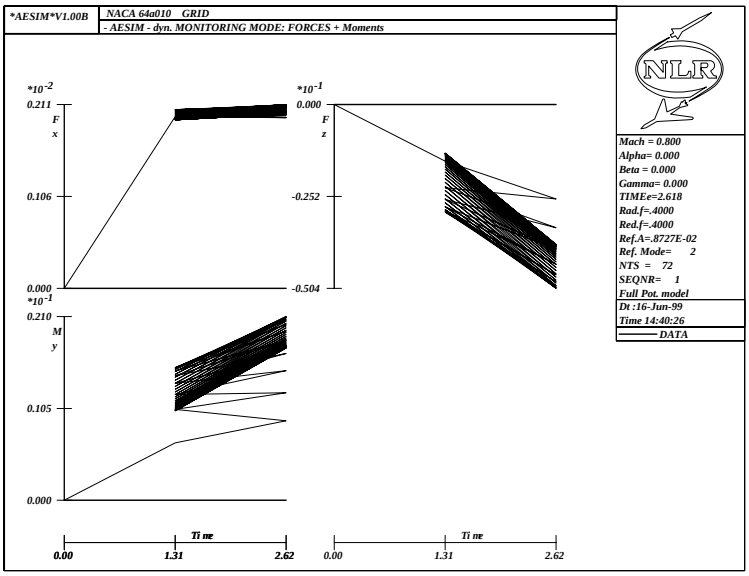

Fig. 43: Response signals of forces during dynamic simulation on NACA64A010 airfoil with the 2-sample scheme at $M_\infty = 0.8$ and$k = 0.2$ on a fine grid with H5U updating.

[3] Starting at k =0.8 it was not possible to obtain a converged solution with the chosen time step and H5U strategy at the higher frequencies. This needs further investigations.

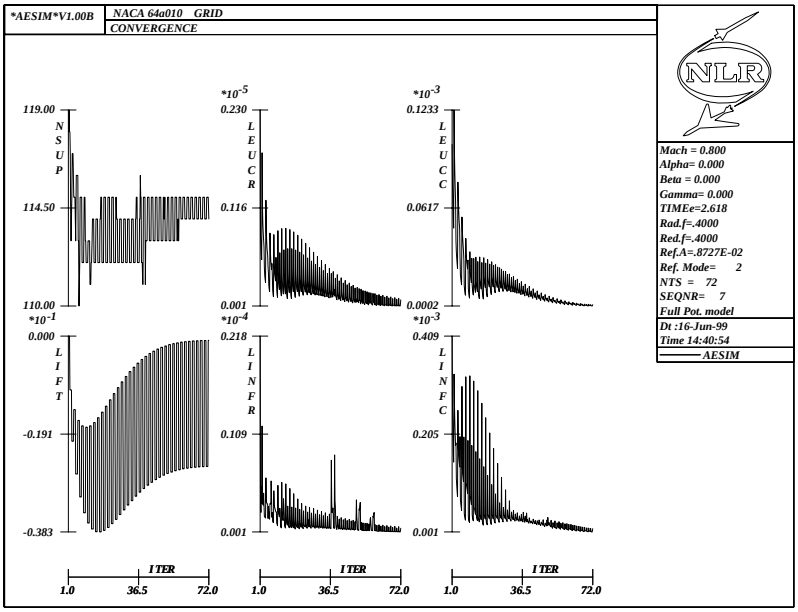

Fig. 44: Convergence characteristics during dynamic simulation on NACA64A010 airfoil with the 2-sample scheme at $M_\infty = 0.8$ and$k = 0.2$ on a fine grid with H5U updating.

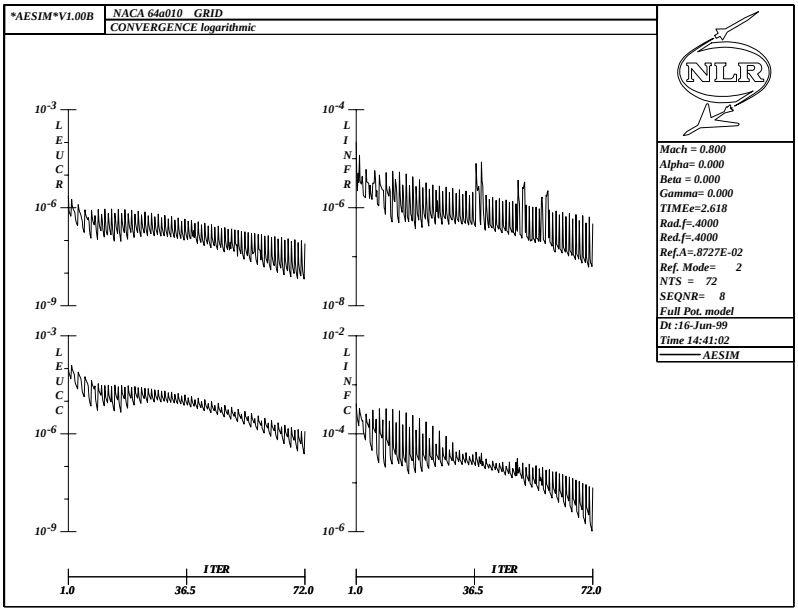

Fig. 45: Convergence characteristics during dynamic simulation on NACA64A010 airfoil with the 2-sample scheme (log scale) at $M_\infty = 0.8$ and$k = 0.2$ on a fine grid with H5U updating.

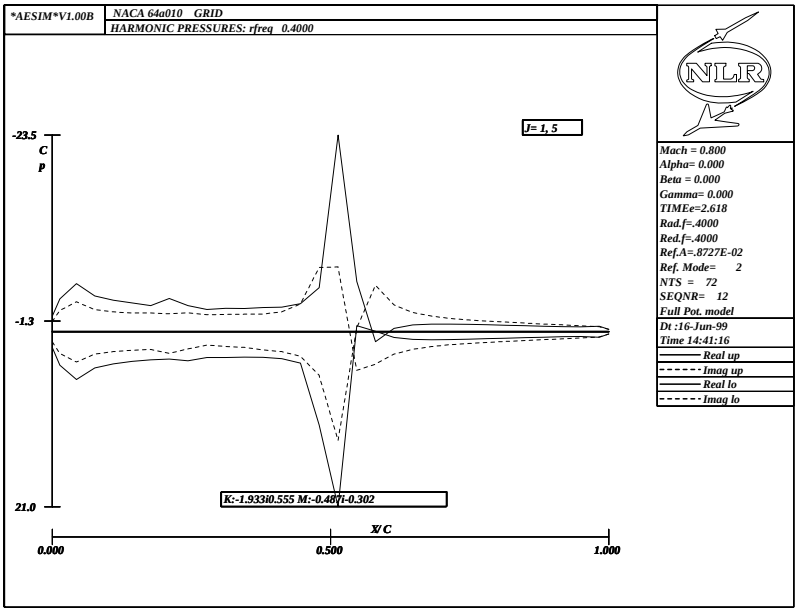

Fig. 46: Harmonic pressure coefficient distributions on NACA64A010 airfoil with the 2-sample scheme at $M_\infty = 0.8$ and$k = 0.2$ on a fine grid with H5U updating.

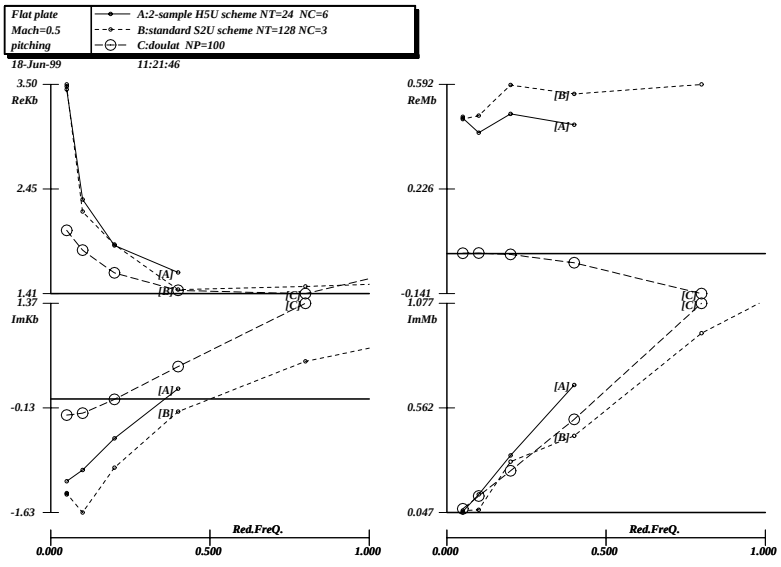

Fig. 47: Comparison of lift and moment coefficients on pitching NACA64A010 at $M_\infty = 0.8$.

6.3 Wing-tail model

In order to demonstrate the ability of the 2-sample scheme to deal with a 3-D multi-surface the unsteady AGARD planar wing-tail configuration with the tail in the plane of the wing has been considered.

The geometry of the wing and tail consists of planar quadrilaterals and symmetric displacement modes of the configuration which are defined in many references and also in [HE94]. The outline of the geometries and the vibration modes are depicted in figure 48.

In [HE94] results have been presented on a coarse grid with a comparable spacing to what is acceptable for lifting surface methods. The grid which is also applied in this study contains 43x20x27 nodes with 10x10 nodes on each side of the two surfaces! Unsteady calculations were performed at $M_\infty = 0.8$ and k=0.5 in wing twisting (tail fixed). It was also concluded that the application of 256 time steps with S2U updating during 3 periods on the current grid results in a 3 digit accuracy and that the unsteady pressure results compared reasonably well to a panel method result.

The results consist of:

Figures 49..52 Simulation using 8 cycles with 32 time steps per cycle at k=0.5 with H5U updating. In figures 49 and 50 the development of the forces for the 2-sample scheme is presented. The latter figure shows the generalized force Q11. It should be noted that only the development of the two samples is shown!. The convergence is rapid. After a few iterations the level is already set. Convergence characteristics are shown in figures 51 and 52.

Figure 53 A comparison between several methods is shown in figure 53. The figure shows results previous obtained with AESIM [HE94] and GUL and results of the 2-sample scheme versus number of iterations and time step [2x4, 2x8, 4x16 and 8x32 (cycles x$\frac{steps}{CYCLE}$]. The following observations can be made (note the scales).

- The convergence is fast, About 30 iterations suffice.
- The CFD data is in agreement.
- There is a large difference between the GUL data and the CFD data which has been discussed in [HE94].

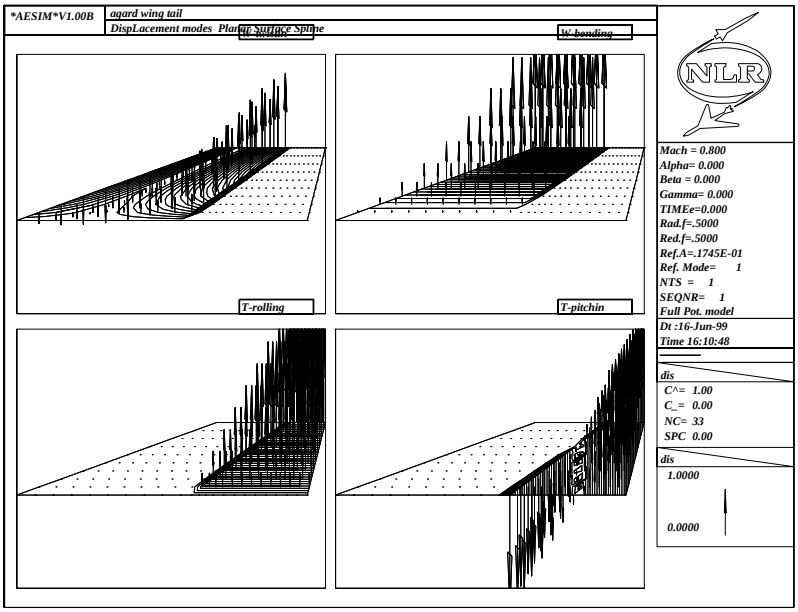

Fig. 48: Outline of planform and vibration modes on AGARD wing-tail configuration.

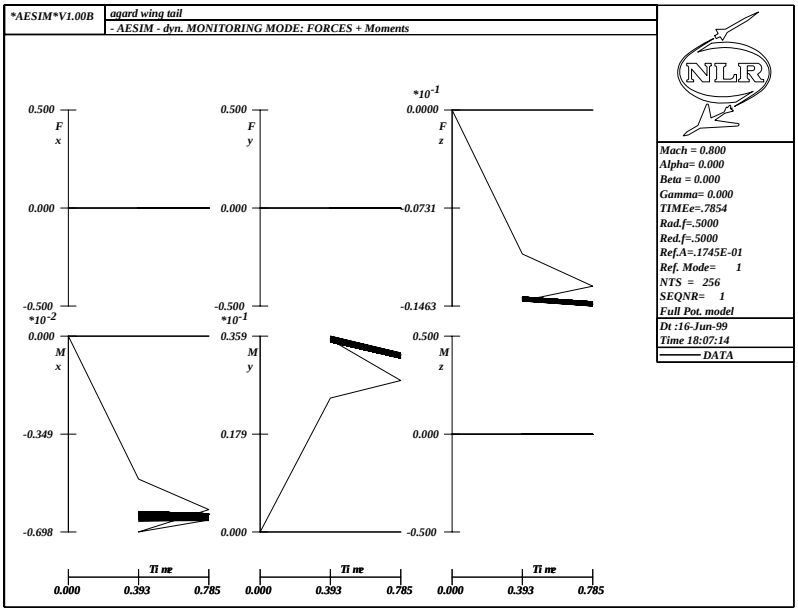

Fig. 49: Response signals of forces during dynamic simulation on wing-tail configuration with the 2-sample scheme at $M_\infty = 0.8, k = 0.5$ and H5U updating.

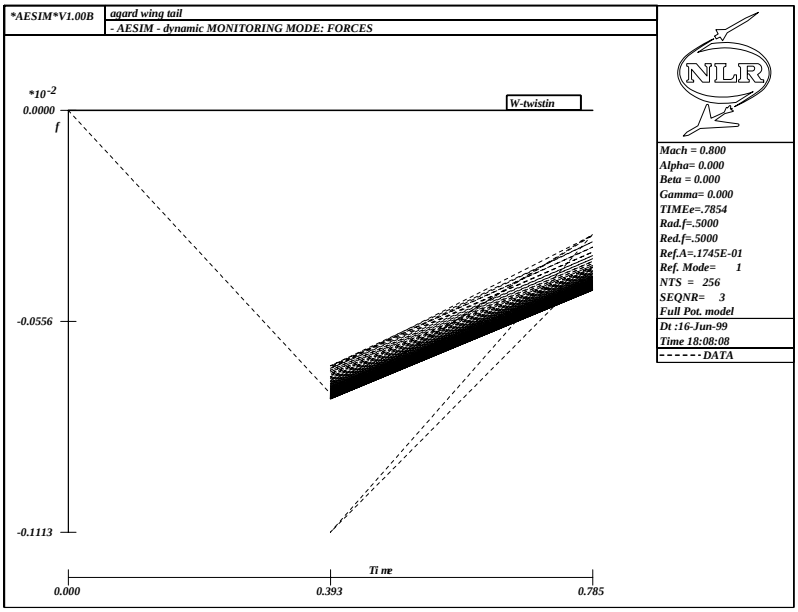

Fig. 50: Response signals of generalized force Q11 during dynamic simulation on wing-tail configuration with the 2-sample scheme at $M_\infty = 0.8, k = 0.5$ and H5U updating.

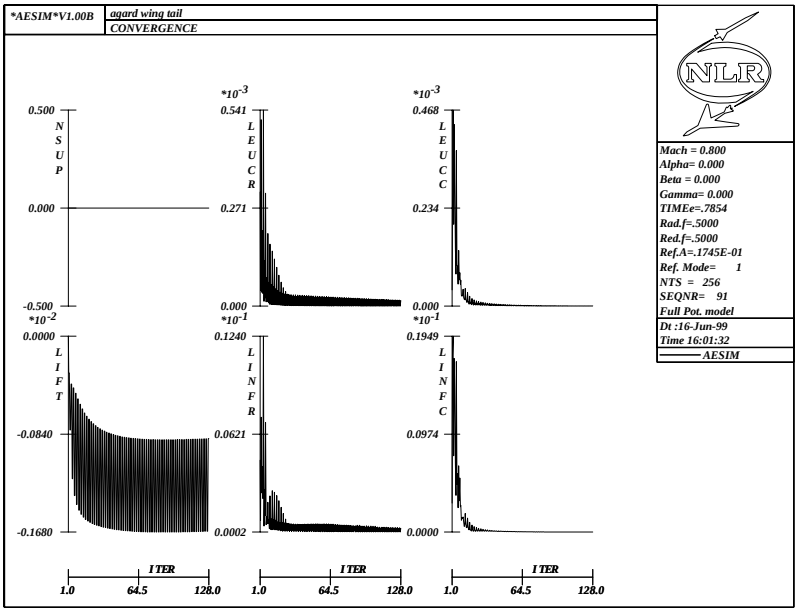

Fig. 51: Convergence characteristics during dynamic simulation on wing-tail configuration with the 2-sample scheme at $M_\infty = 0.8, k = 0.5$ and H5U updating.

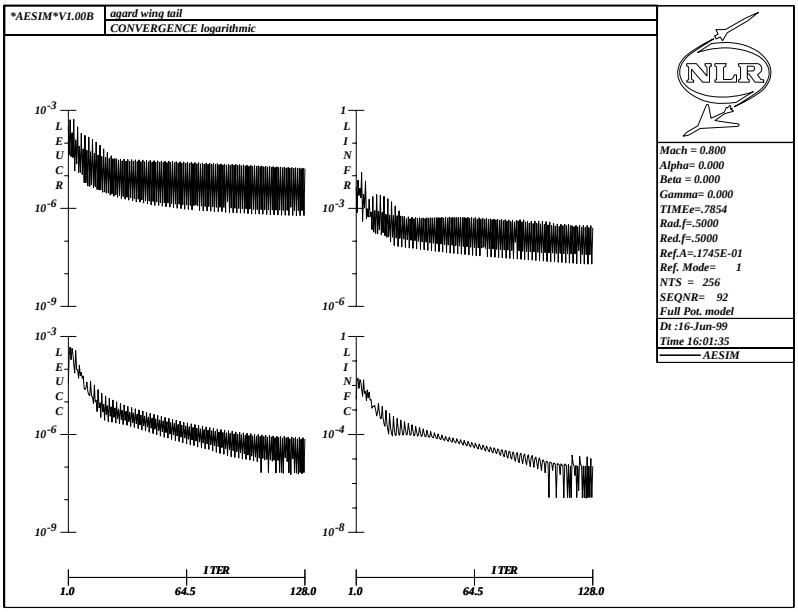

Fig. 52: Convergence characteristics during dynamic simulation on wing-tail configuration with the 2-sample scheme (log scale) at $M_\infty = 0.8, k = 0.5$ and H5U updating.

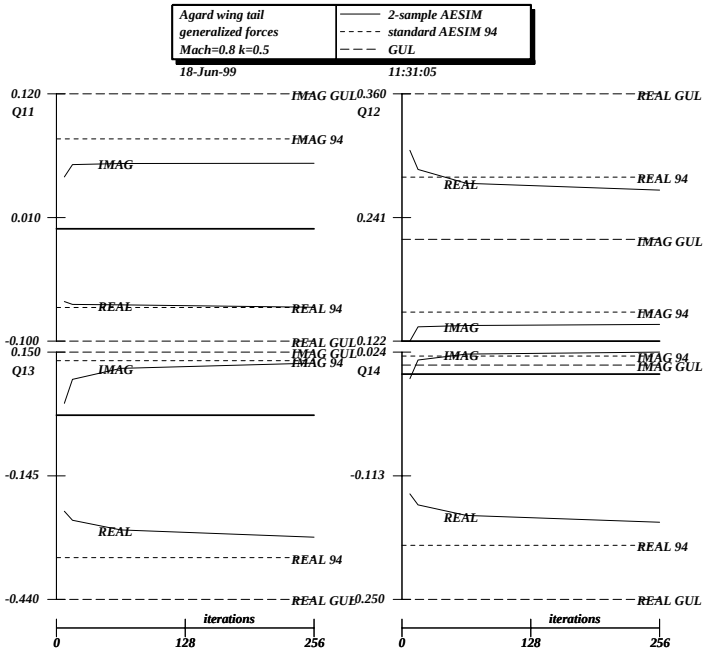

Fig. 53: Comparison of generalized forces on AGARD wing-tail configuration at $M_\infty = 0.8$ and $k = 0.5$.

7 Conclusions

In this paper recently developed approaches to temporal integration and analysis in aeroelasticity have been discussed.

The formulation of the $\frac{[1]\ sample}{cycle}$ and $\frac{[2]\ samples}{cycle}$ concepts for obtaining harmonic and diverging data from time-simulation CFD methods has been presented.

Experience with the presented temporal integration methods in recent applications and ongoing developments led to the following observations:

- The schemes have been applied with good results.
- The schemes are efficient for large time step simulations and relatively low frequencies.
- The schemes are inefficient for small time step simulations and relatively high frequencies and need to be improved.
- The schemes have shown good promise for increasing the applicability of time-accurate CFD methods for obtaining frequency domain data.

References

EHS98. B.G.J. Eussen, M.H.L. Hounjet, and M.W. Soijer. Comprehensive time analysis in aeroelastic simulations. ICAS-98-4.3.3, May 1998.

Fis. P.E. Fischer. Projection Techniques for iterative solution of AX=b with successive Right-Hand Sizes. ICASE report.

FNW97. B. Franzen, B. Nilsson, and B. Winzell. Experience with unsteady aerodynamics computation for saab aircraft. AGARD, Report-822,15.1-15.10, 1997.

HE91. M. H. L. Hounjet and B. J. G. Eussen. Beyond the frequency limit of time-linearized methods. NLR TP91216 U, June 1991.

HE92. M.H.L. Hounjet and B.J.G. Eussen. Prospects of time-linearized unsteady calculation methods for exponentially diverging motions in aeroelasticity. AIAA Paper 92-2122, AIAA, April 1992.

HE94. M.H.L. Hounjet and B.J.G. Eussen. Outline and application of the NLR aeroelastic simulation method. ICAS Paper 94-5.8.2, ICAS, September 1994.

HES97. M.H.L. Hounjet, B.G.J. Eussen, and M.W. Soijer. Analysis of Computational Aeroelastic Simulations by Fitting Time Signals. Proceedings of CEAS International Forum on Aeroelasticity and Structural Dynamics, Rome, Volume 3, June 1997.

Hou85. M.H.L. Hounjet. A field Panel/finite difference method for potential unsteady transonic flow. *AIAA Journal*, 23(4):537–545, April 1985.

Hou86. M.H.L. Hounjet. Application of diverging motions to calculate loads for oscillating motions also as *How to make your aerodynamics in flutter calculations cheaper*, NLR MP 85056 U, August 1985. *AIAA Journal*, 24(10):1723–1725, October 1986.

Hou89. M.H.L. Hounjet. Calculation of unsteady subsonic and supersonic flow about oscillating wings and bodies by new panel methods. NLR Report TP 89119 U, NLR, 1989.

Hou90. M.H.L. Hounjet. Hyperbolic grid generation with BEM source terms. NLR-TP 90334-U, NLR, 1990.

Mor97. G.D. Mortchéléwics. Application des Equations de Euler Linéarisées au Flottement. AGARD, Report-822,5.1-5.7, 1997.

PH97. B.B. Prananta and M.H.L. Hounjet. Large Time Step Aero-Structural Coupling Procedures for Aeroelastic Simulation. International Forum on Aeroelasticity and Structural Dynamics, Ro, 1997.

PHZ98. B.B. Prananta, M.H.L. Hounjet, and R.J. Zwaan. Two-dimensional transonic aeroelastic analysis using Thin-Layer Navier-Stokes method. *Journal of Fluids and Structures*, 12:655–676, 1998.

Pra99. B.B. Prananta. *Physical and Numerical Aspects of Aeroelastic Simulations*. Dissertation, Technische Universiteit Delft, Delft, 1999.

SS86. Y. Saad and M.H. Schultz. A generalized minimum residual algorithm for solving non-symmetric linear systems. SIAM J.Sci.Stat.Comp. Vol 7, pp 856-869, 1986.

Yat88. C. Yates. AGARD Standard Aeroelastic Configurations for Dynamic Response I-Wing 445.6. AGARD Report No. 765, 1988.